A NOVEL CONTROL SCHEME FOR HARMONIC COMPENSATION IN RENEWABLE ENERGY INTEGRATED SYSTEM

A PROJECT REPORT

submitted by

SREELEKSHMI S
(Reg. No. TKM20EEII19)

to

the APJ Abdul Kalam Technological University
in partial fulfillment of the requirements for the award of the Degree

of

Master of Technology
in
Electrical and Electronics Engineering

with specialisation in

Industrial Instrumentation and Control

Department of Electrical and Electronics Engineering
TKM College of Engineering
Kollam - 691 005
KERALA

JULY 2022

DECLARATION

I undersigned hereby declare that the project report entitled "**A Novel Control Scheme for Harmonic Compensation in Renewable Energy Integrated System**", submitted for partial fulfillment of the requirements for the award of degree of Master of Technology in Electrical and Electronics Engineering with specialisation in Industrial Instrumentation and Control, of the APJ Abdul Kalam Technological University, Kerala is a bonafide work done by me under supervision of *Prof. Thasneem A* and *Dr. Mathew P Abraham*, Assistant Professor, Department of Electrical and Electronics Engineering. This submission represents my ideas in my own words and where ideas or words of others have been included. I have adequately and accurately cited and referenced the original sources. I also declare that I have adhered to ethics of academic honesty and integrity and have not misrepresented or fabricated any data or idea or fact or source in my submission. I understand that any violation of the above will be a cause for disciplinary action by the institute and/or the University and can also evoke penal action from the sources which have thus not been properly cited or from whom proper permission has not been obtained. This report has not been previously formed the basis for the award of any degree, diploma or similar title of any other University.

Kollam
July 01, 2022

SREELEKSHMI S

DEPARTMENT OF ELECTRICAL AND ELECTRONICS ENGINEERING

TKM COLLEGE OF ENGINEERING

KOLLAM - 691 005

CERTIFICATE

This is to certify that the report entitled " **A Novel Control Scheme for Harmonic Compensation in Renewable Energy Integrated System** " submitted by **SREELEKSHMI S** , **(Reg. No. TKM20EEII19)** of fourth semester to the APJ Abdul Kalam Technological University in partial fulfillment of the requirements for the award of the Degree of Master of Technology in Electrical and Electronics Engineering with specialisation in Industrial Instrumentation and Control, is a bonafide record of the project work done by her under our guidance and supervision. This report in any form has not been submitted to any other University or Institute for any purpose.

Prof. Thasneem A
Project Supervisor
Assistant Professor
Department of EEE
TKM College of Engineering

Dr. Mathew P Abraham
Project Supervisor
Assistant Professor
Department of EEE
TKM College of Engineering

Prof. Shanavas T N
PG Coordinator
Associate Professor
Department of EEE
TKM College of Engineering

Dr. Sabeena Beevi K
Head of the Department
Associate Professor
Department of EEE
TKM College of Engineering

Prof. Sumayya Jaleel
Project Coordinator
Assistant Professor
Department of EEE
TKM College of Engineering

Acknowledgement

A lot of effort and hard work has been put into this project in course of its presentation. However, it would not have been possible without the kind support and help of many individuals and other sources. I would like to extend my sincere thanks to all of them. I take this opportunity to express my deep sense of gratitude and sincere thanks to all who helped me to complete this project report successfully.

I express my sincere thanks to *Dr. T A Shahul Hameed*, Principal, TKM College of Engineering for his encouragement in completion of my project.

I thank *Dr. Sabeena Beevi K*, Head of the Department, Department of Electrical and Electronics Engineering, *Dr. Imthias Ahamed T P*, Professor, Department of Electrical and Electronics Engineering and *Prof. Shanavas T N*, PG Coordinator, Department of Electrical and Electronics Engineering for their support and cooperation.

I am greatly thankful to my Project supervisor, *Prof Thasneem A*, Assistant Professor and *Dr. Mathew P Abraham*, Assistant Professor, Department of Electrical and Electronics Engineering for their supervision, assistance and helpful suggestions.

I am deeply indebted to *Prof. Sumayya Jaleel*, Assistant Professor, Project Coordinator and *Prof. Amal A*, Assistant Professor, Department of Electrical and Electronics Engineering, for their excellent guidance, positive criticism and valuable comments.

Finally I thank my parents and friends near and dear ones who directly and indirectly contributed to the successful completion of my project.

SREELEKSHMI S

Abstract

Non-linear loads are frequently used in both domestic and industrial applications. A non-linear load connected to the grid produces currents with harmonic content. The voltage and current of the grid are lowered in quality by these harmonics. A Proportional Integral-modified reduced order generalized integrator-based frequency-locked loop (PI+MROGI-FLL) is developed for controlling the interfacing inverter to mitigate the harmonics. The PI+MROGI-FLL is designed to evaluate the three-phase reference currents by extracting the fundamental constituents from the load currents. It offers many benefits, including improved harmonic mitigation, adaptive frequency and phase, grid synchronisation, and minimal computational burden. The suggested controller is modelled in MATLAB/Simulink using both a PV system and a hybrid system. The proposed controller's performance is compared with that of existing conventional controllers. In comparison to other controllers, the PI+MROGI controller exhibits higher harmonic mitigation capability.

Contents

List of Tables

List of Figures

Abbreviations

DER	Distributed Energy Resources
DG	Distributed Generation
DSOGI	Dual Second Order Generalized Integrator
INC	Incremental Conductance
ISOGI	Improved Second Order Generalized Integrator
MPPT	Maximum Power Point Tracking
MROGI	Modified Reduced Order Generalized Integrator
PCC	Point of Common Coupling
PEMFC	Proton Exchange Membrane Fuel Cell
PIROGI	PI+Reduced Order Generalized Integrator
ROGI	Reduced Order Generalized Integrator
SOGI	Second Order Generalized Integrator
SRF	Synchronous Reference Frame

Notations

f_{sw}	Switching Frequency, Hz
I'	Estimated current amplitude, A
I'_{α}, I'_{β}	$\alpha\beta$ constituents of current, A
I_{net}	Net current, A
I_{rabc}	Reference current, A
I'_{θ}	Estimated current phase, A
K'_r	Modified controller Gain
K_r	Gain of ROGI controller
K_s	Gain of SOGI controller
λ	Integral gain of controller
P_g	Grid Power, kW
V_g	Grid Voltage, V
V_{iabc}	In-phase component of UVT, V
V_{pabc}	Grid voltage at PCC, V
V_{qabc}	Quadrature component of UVT, V
V_t	Unit Vector Template, V
ω'	Estimated frequency, Hz
Z_l	Line Impedance

Chapter 1

INTRODUCTION

1.1 General Background

The growing concern about environmental pollution and the scarcity of fossil fuels has raised interest in renewable energy sources like solar, fuel cells, and wind power, which are clean, pollution-free, and renewable. On the other hand, because of their sporadic nature, these resources are less effective over time than non-renewable ones. During low sun hours, for example, PV output dwindles to the point where it can no longer match the load requirement. Integration with the utility grid can improve the overall performance of Distributed Energy Resources (DER)[3].

The output of renewable sources like solar cells and fuel cells is dc voltage, whereas the grid has a constant ac voltage. Conversion from AC to DC is crucial. Grid-connected inverters are therefore essential parts of distributed generating systems. Due to the power electronic equipment switching in these inverters, harmonics are produced at the Distributed Generating (DG) output. For instance, the inverter may experience high-frequency switching under low solar energy irradiance levels, which causes a severely distorted current injection into the distribution network. These harmonics include high-frequency components that are multiples of the inverter's carrier frequency. At the inverters' output, interfacing inductors are used to cut down the harmonics. These filters have the capacity to cause a harmonic resonance in the system if not constructed properly.

Harmonics are also produced by nonlinear loads, point of common coupling (PCC), and utility loads operating in the system, at multiples of the power grid frequency. Utility grid

currents are impacted by the presence of nonlinear load currents, which causes grid voltage disturbances such voltage flickering, blackouts, imbalance, distortion, and overheating or device failure. To ensure that consumers receive satisfactory power quality, utility companies must keep the system's harmonics levels below the permitted thresholds set by grid regulations. Shunt active power filters are frequently used to reduce the current harmonics brought on by non-linear loads[4]. The performance of an active filter is significantly influenced by the reference current generation method.

1.2 Motivation

Because of the digitalisation and increased usage of electronic devices in facilities, such as computers and other digital machinery, the relevance of power quality has grown. As a significant underutilised source of cost savings and economic benefit, poor power quality has emerged as a serious issue in many industrial plants. In the worst situation, it might endanger human life in very sensitive areas and mission-critical applications, like hospitals.

Poor power quality can result in a variety of detrimental and expensive effects. Without realising it, it can be wasting resources and decreasing production. On the other hand, the benefits of power quality correction might be numerous and long-lasting, improving the operations. Good power quality reduces costs and uses less energy. Lower energy prices and reactive power tariffs result in immediate savings for consumers. By averting situations like equipment damage and early ageing, production loss, and data and work loss, indirect savings can be realised. Therefore the need for greater power quality is becoming increasingly crucial for businesses interested in energy efficiency and ongoing management.

1.3 Objectives

The objectives of the work include the following,

1. To design a novel control scheme for the harmonic mitigation in a PV integrated system.
2. To compare the performance of the proposed controller with the existing control techniques.
3. To analyse the performance of the controller in a hybrid system.

1.4 Organisation of the report

The structure of the entire thesis is as follows. There are six chapters in it. A brief introduction, motivation, and the objectives are included in Chapter 1. The literature study of various control measures to lessen current harmonics is covered in Chapter 2. Chapter 3 deals with the overall design of the system. Design and implementation of various controllers used to mitigate harmonics is included in Chapter 4. The simulation results of the different controllers in PV integrated and hybrid system is given in Chapter 5. Comparison of the controllers using the simulation result is also included. The overall conclusion and future scopes are discussed in chapter 6.

Chapter 2

LITERATURE REVIEW

2.1 Introduction

The control mechanisms employed in grid-connected renewable energy systems for improving power quality are described in this chapter in the light of prior research and practises.

2.2 Literature Survey

Several control approaches for APF have been implemented in the last two decades, including PQ theory, Synchronous Reference Frame (SRF) theory, Self-Tuning Filter (STF), Second Order Generalized Integrator (SOGI)[5], Improved Second Order Generalized Integrator (ISOGI)[6], Dual Second Order Generalized Integrator (DSOGI), Reduced Order Generalized Integrator (ROGI), PI Reduced Order Generalized Integrator (PI ROGI)[7], Modified Reduced Order Generalized Integrator (MROGI).

Synchronous reference frame theory is employed in [8]. The paper uses Park transformation to operate. To determine the angular location, use a phase lock loop. To distinguish between the fundamental and harmonic components of the instantaneous load, the measured 3-phase source voltage and current are simultaneously converted into their respective 2-phase components. The separation uses a low pass filter. However, it has a number of drawbacks, such as a heavy computational burden and time delay brought on by reliance on numerical filters and the need for an additional PLL circuit.

Paper [9] makes use of the instantaneous reactive power theory (PQ theory). It uses Clarke transformation to function. The observed 3-phase source current and voltage are converted into the corresponding 2-phase components simultaneously. Calculated active and reactive powers are separated into their fundamental and harmonic components using a low pass filter. However, because of its reliance on numerical filters, it has a number of drawbacks, including a heavy computational burden and a time delay.

Paper [10] generate reference current using a modulated hysteresis current controller and a self-tuning filter, no phase delay as a result. The benefit is that it doesn't need a PLL, low pass filter, or high pass filter. Its drawbacks include significant computational burden and the need for meticulous gain parameter calibration for STF.

The reference current is produced in [11], [12] using a second order generalised integrator. The angular frequency is measured using PLL. Better harmonic and inter-harmonic compensation, tracking precision, and quicker reference signal recognition are all features of this system. But only single-phase systems can use single SOGI. Three SOGIs are needed for 3-phase applications. It is unable to discriminate between the fundamental signal's positive and negative sequence components.

In [13], the 3-phase system is converted to a 2-phase system, and the reference current is produced by a double SOGI. Better harmonic and inter-harmonic compensation, tracking precision, and quicker reference signal recognition are all features of this system. However, it is unable to tell the fundamental signal's positive and negative sequence components apart. For this, they employ the positive-negative sequence calculation block.

Reduced Order Generalised Integrator (ROGI) refers to a Second Order Generalised Integrator that has been reduced to a Single Order Generalised Integrator in [14], [15]. Using a first order complex vector filter, it can immediately discriminate between the positive and negative sequence components of the fundamental signal. It takes less computational time and avoids the additionally required transformations. It simply makes use of direct feedback on estimated inaccuracy. This prevents from controlling the closed loop system's imaginary eigenvalues.

In [16], ROGI is changed to a modified version called the Modified Reduced Order Generalized Integrator, which uses cross feedback in addition to direct feedback to address ROGI's shortcomings. It requires less computing time and does away with the extra transformations that are needed.

2.3 Conclusion

In light of existing research and practises, this chapter explored the characteristics, benefits, and limitations of several control techniques used in grid-connected renewable energy systems to improve power quality. Modified ROGI controller have the ability to distinguish positive and negative sequence components and also control the imaginary eigen values of the closed loop system. This enables the system to improve the harmonic mitigation capability and give a faster response.

Chapter 3

SYSTEM DESIGN

3.1 Introduction

The basic structure of the system includes PV array, Maximum Power Point Tracking, fuel cell, Boost converter, inverter etc. A brief introduction and mathematical modelling of these components are discussed in this chapter.

3.2 Basic Structure of the System

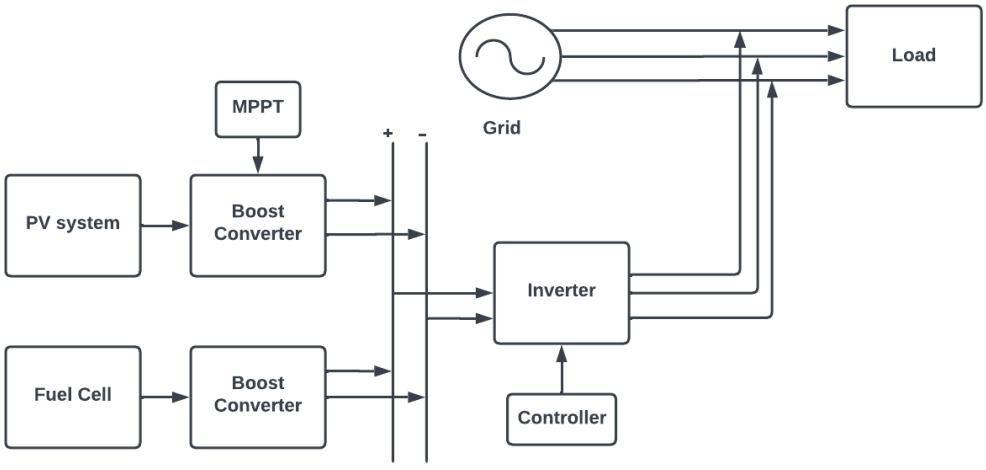

Figure 3.1: Block diagram of the system.

The system under discussion is a three-phase integrated renewable energy system[17]. Two green energy sources are used by the system. The first is a solar panel, while the second

is a fuel cell. It is the two-stage structure of the system, specifically the DC-DC and DC-AC conversions. The boost converter uses the solar PV and fuel cell power and carries out two tasks. The first is it increase the power output of the source, secondly it Boost and regulate the DC output voltage. The boost converter's DC input is taken by the DC-AC conversion stage, which then injects it as AC power into the grid. To eliminate higher frequency harmonics from the inverter output, an inductive filter is positioned in between the inverter and the grid.

3.3 PV Array

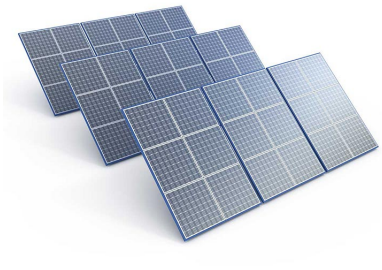

Figure 3.2: PV Array[1]

A solar cell, sometimes referred to as a photovoltaic cell, is an electrical device that converts light energy directly into electricity by utilising the photovoltaic effect, a physical and chemical phenomenon. It is a particular kind of photoelectric cell, which is characterised as a component whose electrical characteristics, such as current, voltage, or resistance, vary in response to light[18], [19].

PV systems use solar panels, which are collections of solar cells typically made of silicon and installed on a rigid flat framework. Strings and arrays of solar panels are created by connecting solar panels in series and parallel, respectively. The quantity of DC that solar panels produce determines its rating. Many benefits of using PV systems draw users to them. The key benefits are that sunlight is free and accessible throughout, they don't emit any greenhouse gases or noise, and grid-connected PV systems can lower utility rates.

The specifications of the Photovoltaic system is given in Table 3.1. Figure 3.3 shows the P-V and V-I curve of the PV system.

Table 3.1: Parameters of PV System

Parameter	Value
Maximum Power, P_{max}	32 kW
Irradiance, I_r	$1000W/m^2$
Temperature,T	25°C
Voltage at Maximum Power, V_{max}	500 V
Current at Maximum Power, I_{max}	66.15 A
Open Circuit Voltage, V_{OC}	620 V
Short Circuit Current, I_{SC}	70.56 A

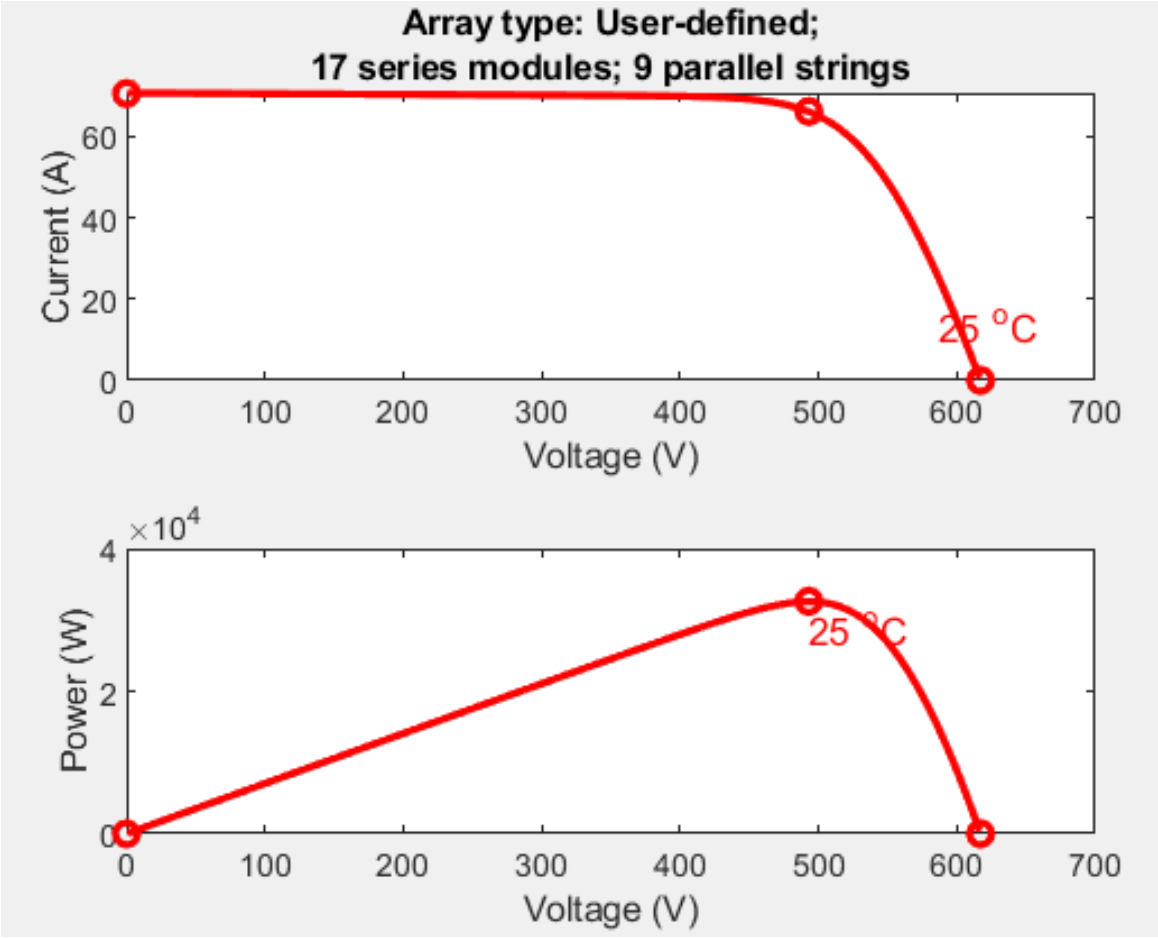

Figure 3.3: IV and PV characteristics of solar panel.

3.4 Maximum Power Point Tracking

In order to generate solar power, a solar panel's power output must be maximised. Solar cells cannot supply constant electricity because of their non-linear behaviour. Additionally, the power characteristics of the solar cell are impacted over time by external variables including temperature and irradiance. A solar cell's output voltage needs to be monitored to be close to the maximum power point under varying irradiance and temperature conditions in order to produce the maximum power. Since the PV array generates the greatest amount of power during regular daylight hours and least power at other hours, MPPT can increase a solar cell's overall efficiency.

MPPT algorithms are becoming more popular due to their high efficiency and improved version for obtaining the most power from the solar cell. For MPPT controllers, a variety of algorithms are available. Perturbation and observation (P&O), incremental conductance technique (INC), and fuzzy logic controller method are the most frequent. Voltage and current sensors are used by INC MPPT to determine the output voltage and current of the PV array. The error brought on by a change in irradiance is reduced because the voltage and current are detected concurrently.

The incremental conductance algorithm finds the slope of the P-V curve, and the Maximum Power Point (MPP) is tracked by searching the peak of the P-V curve. For MPPT, this technique uses the instantaneous conductance $\frac{I}{V}$ and the incremental conductance $\frac{dI}{dV}$. The P-V array power curve has a slope of zero at the MPP, increasing to the left of the MPP, and decreasing to the right of the MPP. The basic equations governing the INC method are as follows:

$$\begin{cases} \frac{dI}{dV} = -\frac{I}{V} & \text{at MPP} \\ \frac{dI}{dV} > -\frac{I}{V} & \text{at left of MPP} \\ \frac{dI}{dV} < -\frac{I}{V} & \text{at right of MPP} \end{cases} \tag{3.1}$$

where,

I= PV array output current

V= PV array output voltage

The following flow chart will help to understand the INC method.

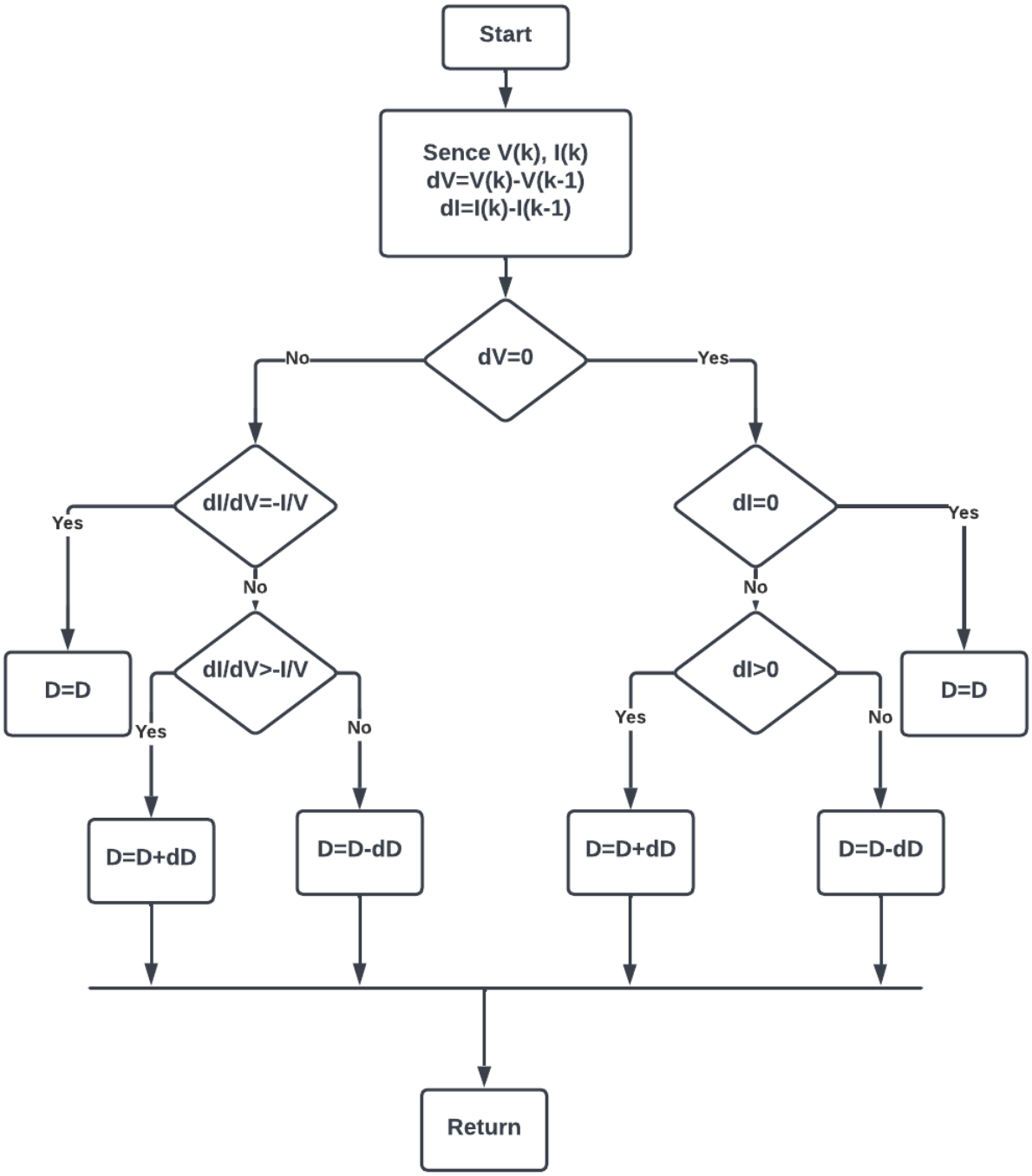

Figure 3.4: Incremental Conductance MPPT Algorithm.

3.5 Fuel Cell

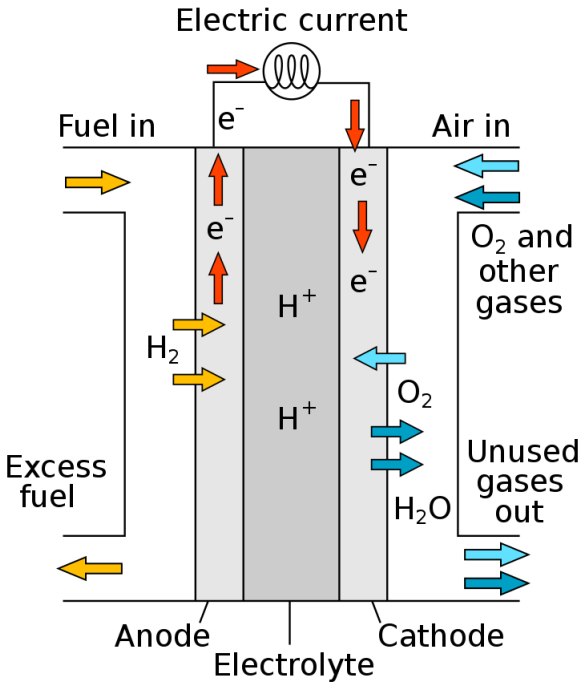

Figure 3.5: Fuel Cell[2]

While depending only on solar energy may seem like the most efficient approach to generate energy, many locations across the world simply do not receive enough useful solar hours since the sun does not shine all day. In order to provide the ideal sustainable energy solution, a fuel cell and solar panel are coupled[20], [21], [22].

Instead of using combustion to produce energy, a fuel cell uses an electro-chemical reaction. Hydrogen and oxygen are mixed to produce electricity, heat, and water in a fuel cell. Power generated by fuel cell devices is safe, effective, dependable, and silent. In contrast to batteries, which need to be periodically recharged, fuel cells may keep producing energy as long as a fuel supply is available.

Anode, cathode, and a membrane containing the electrolyte make up a fuel cell. In a conventional fuel cell, oxygen and hydrogen are passed through the cathode while hydrogen is passed through the anode. A catalyst divides the hydrogen molecules into protons and electrons at the anode location. The electrons are driven through a circuit while the protons are propelled through the porous electrolyte membrane, creating an electric current and extra heat. At the cathode, oxygen, protons, and electrons react to form water molecules.

Table 3.2: Fuel cell parameters

Parameter	Value
Maximum Power, P_{max}	50 kW
Nominal Voltage, V_{nom}	625 V
Nominal Current, I_{nom}	80 A
Operating Temperature, T	65°C

Since they don't have any moving parts, fuel cells are incredibly reliable and operate quietly. Fuel cells are substantially more efficient than conventional energy generation techniques like steam turbines and internal combustion engines because they produce electricity through chemistry rather than combustion.

A Proton-Exchange Membrane Fuel Cell (PEMFC) is used along with the solar panel as renewable source. PEMFC has many advantages. They use Solid electrolyte which reduces corrosion & electrolyte management problems. They operate at Low temperature. They have Quick start-up and load following capability. Table 3.2 shows the parameters of the fuel cell.

3.6 Boost Converter

Applications involving renewable energy frequently use boost converters. Since they are sporadic, it is essential to make the entire system effective in order to mitigate the effects of sporadicity. A boost converter aids in improving a system's overall efficiency. Low voltage to high voltage conversion is accomplished via a boost converter. Additionally, it regulates output power.

The two-stage integrated renewable energy generation system needs a constant current injection in the DC-link, which is the output capacitor of the boost converter. Constant current injection makes sure that the output voltage swings barely at all and that the DC-link voltage fluctuates only slightly. A steady DC voltage input will be provided to the inverter as a result, which is necessary to maximise an inverter's effectiveness and efficiency. A boost converter is also less expensive when compared to other converters.

Figure 3.6 shows a basic boost converter. The diode will be reversed biased during switching on; therefore, the input current will be the same as the inductor current. The voltage across

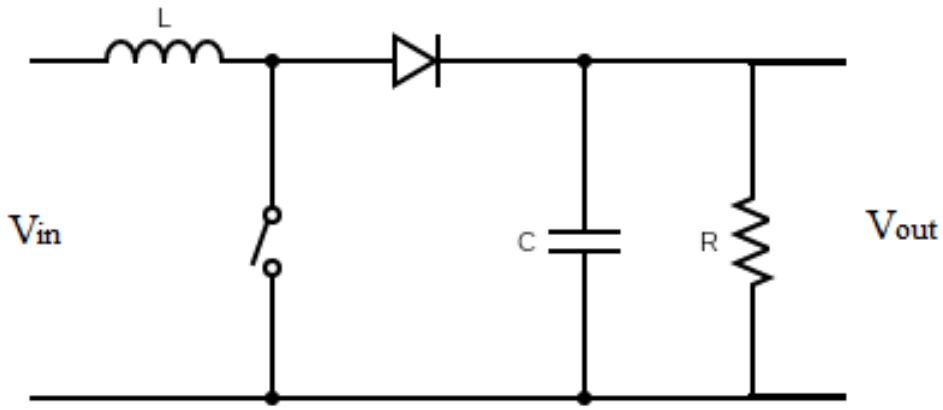

Figure 3.6: Boost Converter.

the capacitor would be the output voltage during the on-interval. The capacitor's value should be large enough to maintain a constant voltage across the load. The inductor discharges in the opposite direction during the off-interval, causing a diode to become forward biased. Therefore, the output voltage V_{out} will be the sum of input voltage V_{in} and inductor voltage. The relationship between the input and output voltages can be ascertained using the volt-sec balance across the inductor. The volt-sec balance predicts that the steady-state voltage across the inductor would be zero for one cycle. The input voltage and output voltage have the following relationships:

$$V_{out} = \frac{V_{in}}{(1-D)} \tag{3.2}$$

The relationship between the output current I_{out} and the input current I_{in} can also be discovered, supposing there are no losses in the circuit.

$$I_{out} = I_{in}(1-D) \tag{3.3}$$

where, D is the duty cycle There are boost converters available in both continuous conduction mode (CCM) and discontinuous conduction mode (DCM). While the inductor current in DCM will be zero and could have interleaved zero inductor current timing, it will be non-zero in CCM.

The two most crucial components of boost converter design are the inductor and capacitor choices. The values of an inductor and a capacitor depend on a variety of variables. In a boost converter design, the primary equation that selects which inductor to employ is

$$Inductance, L = \frac{V_{out}(V_{in} - V_{out})}{f_{sw}\Delta I_{in} V_{in}} \tag{3.4}$$

where, f_{sw} is the switching frequency of boost converter and ΔI_l is the estimated inductor ripple current. For an input voltage of 500 V and an output voltage of 800 V, the D value is found to be 0.375. 65 A is the input current. Five percent of the input current is thought to make up the inductor ripple current. Therefore, 0.115 mH is chosen as the inductance value for the boost converter.

The capacitor we select has a significant impact on the boost converter's overall performance. If not, it could cause oscillations in both active and reactive power toward the grid. It should be big enough to reduce power oscillations toward the grid. In order to increase an inverter's lifespan, it should also lessen DC-link voltage swings. The equation controls the choice of a capacitor value for the boost converter is,

$$Capacitance, C = \frac{I_{out}(V_{in} - V_{out})}{f_{sw}\Delta V_{out} V_{out}} \tag{3.5}$$

where, ΔV_{out} is the estimated capacitor ripple voltage. The 8 V voltage ripple is calculated using a 1 percent ripple assumption. Consequently, 37.5 mF is chosen as the boost converter's capacitance.

3.7 AC System

An alternating current that is frequently utilised in the production, transmission, and distribution of electricity is referred to as three-phase electric power (abbreviated as 3ϕ). It is the most typical way electrical networks utilise to carry power throughout the world, using three wires (or four if you include an extra neutral return line). When three wires are connected in three-phase power, the voltage and current are 120 degrees out of phase. Because it requires less conductor material to transfer a given quantity of electrical power, a three-wire three-phase circuit is typically more cost-effective than an equivalent two-wire single-phase circuit at the same line to ground voltage. The majority of heavy loads, such as big induction motors and other electric motors, are directly powered by three-phase current.

In a symmetric three-phase power distribution system, three wires each carry an alternating current with the same frequency and voltage amplitude in relation to a common reference, but with a phase difference of one third of a cycle (i.e., 120 degrees out of phase) between each.

Table 3.3: Grid parameters

Parameter	Value
Grid Power, P_g	6 kW
Grid Voltage,V_g	230 V
Frequency, f	50 Hz
Line Impedance, Z_l	R= 0.01 Ω, L=1.5 mH

Following equations can be used to represent the three-phase balanced grid.

$$\begin{cases} V_a = V cos(\omega t) \\ V_b = V cos(\omega t - \frac{2\pi}{2}) \\ V_c = V cos(\omega t + \frac{2\pi}{2}) \end{cases} \tag{3.6}$$

These equations represent the three-phase grid voltages having peak voltage V and angular frequency ω.

3.8 Load

Three-phase RLC load is given as the linear load and Six-pulse bridge-type full-wave three-phase uncontrolled rectifier with RL load act as the nonlinear load.A balanced 3-phase, 3-wire supply can be used to power the full-wave rectifier. The circuit for a full-wave 3-phase rectifier is displayed in Figure 3.7.

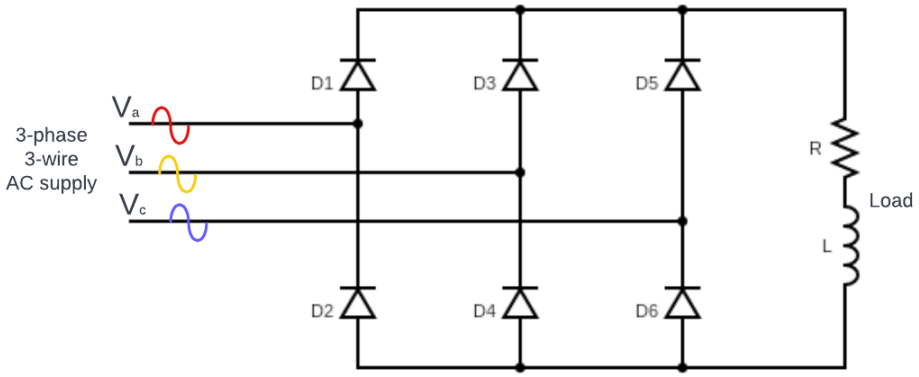

Figure 3.7: Uncontrolled Rectifier with RL Load.

3.9 Conclusion

The system's overall design was covered in this chapter. A brief description and design of each system component is also provided.

Chapter 4

CONTROLLER DESIGN

4.1 Introduction

In this chapter, modelling of the system's controllers is covered. For harmonic mitigation, five distinct controllers have been modelled. The generation of reference current is also described.

4.2 Dual Second Order Generalized Integrator(DSOGI)

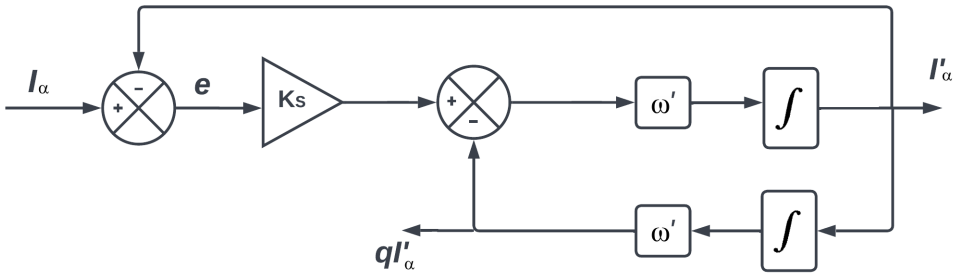

Figure 4.1: Basic Structure of Second Order Generalized Integrator.

Figure 4.1 depicts a SOGI controller's fundamental construction. The computational burden is lowered because of its uncomplicated structure, and the structure is also frequency adaptable. Two sine waves with a 90 degree phase shift are generated as the output signals. The input's band-pass filtered version with a unity gain and zero phase shift at the frequency ω is the first component, I'_α. Second output, qI'_α is the input's low-pass filtered version with a unit gain

and a phase shift of 90° at the frequency of ω[23]. The current's magnitude is determined by

$$A = \sqrt{{I'_\alpha}^2 + q{I'_\alpha}^2} \tag{4.1}$$

Basic equation of SOGI controller is given by,

$$SOGI(s) = \frac{\omega' s}{s^2 + \omega'^2} \tag{4.2}$$

The following is the closed loop transfer function:

$$G_d(s) = \frac{I'_\alpha(s)}{I_\alpha(s)} = \frac{k_s \omega' s}{s^2 + k\omega' s + \omega'^2} \tag{4.3}$$

$$G_q(s) = \frac{I'_\alpha(s)}{I_\alpha(s)} = \frac{k_s \omega'^2}{s^2 + k\omega' s + \omega'^2} \tag{4.4}$$

where, k_s is the SOGI controller gain and ω is the frequency.

Since this controller's tuning is frequency dependent, issues could arise if the grid's frequency fluctuates. As a result, a Frequency Lock Loop (FLL) is used to modify the SOGI controller's resonance frequency value. The primary function of this controller is to instantly filter out the essential component from the load current.

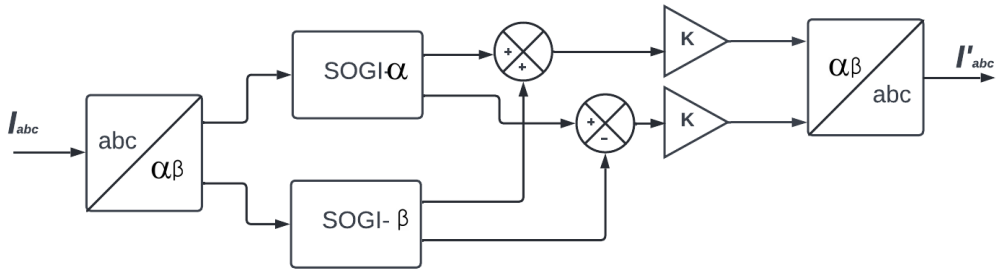

Figure 4.2: Basic Structure of Dual Second Order Generalized Integrator.

The figure 4.2 depicts the DSOGI's fundamental structure. Utilizing the Clarke transformation, the three-phase load current component is changed from three to two phases. The essential components are extracted from two phases separately using dual SOGIs. Clark transformation equation is:

$$I_{abc}(t) = \frac{3}{2} \begin{bmatrix} \frac{2}{3} & 0 \\ -\frac{1}{3} & \frac{\sqrt{3}}{3} \\ -\frac{1}{3} & -\frac{\sqrt{3}}{3} \end{bmatrix} \begin{bmatrix} I_\alpha(t) \\ I_\beta(t) \end{bmatrix} \tag{4.5}$$

4.3 Reduced Order Generalized Integrator (ROGI)

Due to the DSOGI's inability to successfully mitigate lower-order harmonics and reject dc offsets, order of SOGI controller is reduced to a first order controller and hence the name Reduced Order Generalized Integrator (ROGI). The equation for SOGI can be written as,

$$SOGI(s) = \frac{\omega' s}{s^2 + \omega'^2} = \frac{1}{2}\left(\frac{\omega'}{s + j\omega'} + \frac{\omega'}{s - j\omega'}\right) \tag{4.6}$$

where, $\pm j\omega'$ are the system's poles, which explains why SOGI is unable to achieve the basic separation of the grid's positive and negative sequence due to a lack of positive and negative polarity choices.

$$ROGI(s) = \frac{\omega'}{s - j\omega'} \tag{4.7}$$

When ω' equals ω, where ω is the positive synchronous rotating angular frequency, it is possible to distinguish between the positive and negative sequence components of the grid current. A Frequency Locked loop is used to equate ω' and ω.

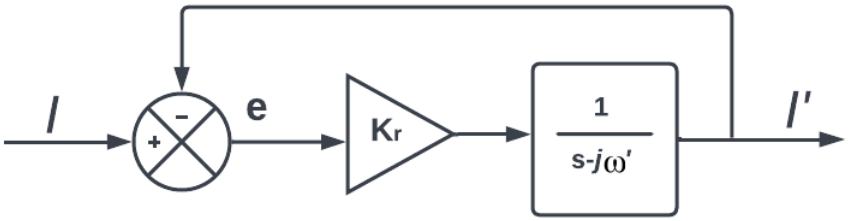

Figure 4.3: Basic Structure of Reduced Order Generalized Integrator

However, when transfer function ROGI(s) contains complex number j, it is difficult to conceptualise it in maths. Therefore, the connection $I_\alpha = jI_\beta$ takes the place of j.

$$I' = \frac{k_r e}{s - j\omega'} \tag{4.8}$$

$$I'(s - j\omega') = k_r e \tag{4.9}$$

Taking Inverse Laplace Transform,

$$\frac{dI'}{dt} = k_r e + I' j\omega' \tag{4.10}$$

$$\frac{dI'_\alpha}{dt} = k_r e_\alpha + I'_\alpha j\omega' \tag{4.11}$$

Substituting for jI'_α,

$$\frac{dI'_\alpha}{dt} = k_r e_\alpha - I'_\beta \omega' \tag{4.12}$$

similarly,

$$\frac{dI'_\beta}{dt} = k_r e_\beta + I'_\beta j\omega' \tag{4.13}$$

Substituting for jI'_β,

$$\frac{dI'_\alpha}{dt} = k_r e_\beta + I'_\alpha \omega' \tag{4.14}$$

The ROGI controller's elaborated construction using the above mentioned equations is shown in figure 4.4. Figure 4.5 depicts the FLL's structural layout. The estimated frequency can be calculated by,

$$\begin{cases} \frac{d\omega'}{dt} = \frac{\lambda}{I'^2}\left[I'_\alpha e_\beta - I'_\beta e_\alpha\right] \\ \qquad = \frac{\lambda}{I'^2}\left[I'_\alpha I_\beta - I'_\beta I_\alpha\right] \end{cases} \tag{4.15}$$

where,

I'= Estimated Current Amplitude

λ=Integral Gain of Controller

k_r= Controller gain

ω'=Estimated Frequency

e_α, e_β= α, β errors of current

$I'_\alpha . I'_\beta$= α, β fundamental constituents of current

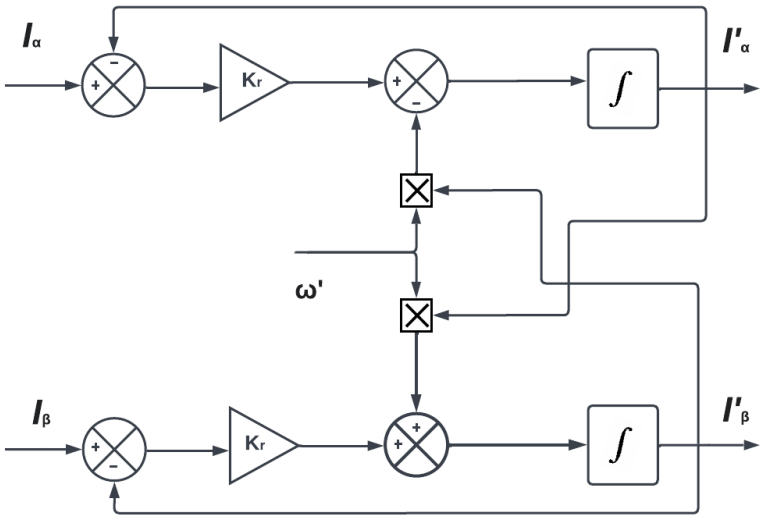

Figure 4.4: Detailed Structure of Reduced Order Generalized Integrator.

Closed loop transfer function of ROGI controller is given by,

$$G_r(s) = \frac{k_r}{(s - j\omega') + k_r} \tag{4.16}$$

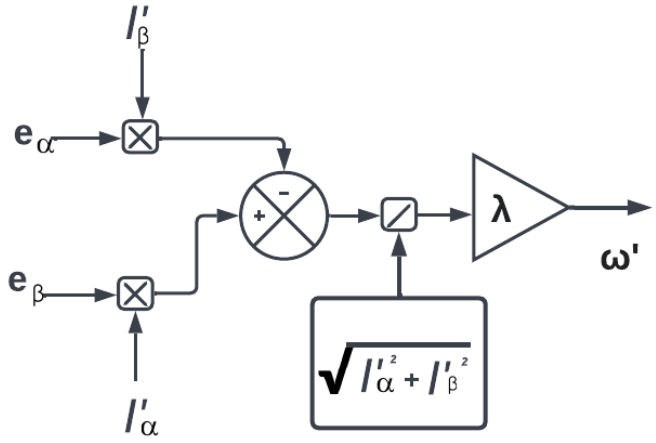

Figure 4.5: Basic Structure of Frequency Locked Loop.

4.4 Modified Reduced Order Generalized Integrator (MROGI)

Only direct feedback of the estimated inaccuracy is used by standard ROGI. This makes it impossible to alter the system's imaginary eigenvalues. To get over the above restriction, ROGI is updated using cross feedback in addition to direct feedback and is called Modified Reduced Order Generalized Integrator(MROGI).

$$I' = \frac{k_r e - k'_r e}{s - j\omega'} \tag{4.17}$$

$$I'(s - j\omega') = k_r e - k'_r e \tag{4.18}$$

Taking Inverse Laplace Transform,

$$\frac{dI'}{dt} = k_r e - k'_r e + I' j\omega' \tag{4.19}$$

$$\frac{dI'_\alpha}{dt} = k_r e_\alpha - k'_r e_\beta + I'_\alpha j\omega' \tag{4.20}$$

Substituting for jI'_α,

$$\frac{dI'_\alpha}{dt} = k_r e_\alpha - k'_r e_\beta - I'_\beta \omega' \tag{4.21}$$

similarly,

$$\frac{dI'_\beta}{dt} = k_r e_\beta + k'_r e_\alpha + I'_\beta j\omega' \tag{4.22}$$

Substituting for jI'_β,

$$\frac{dI'_\alpha}{dt} = k_r e_\beta + k'_r e_\alpha + I'_\alpha \omega' \tag{4.23}$$

where,

k'_r= Modified Controller gain

Figure 4.6 illustrates the detailed design of the MROGI controller utilising the above mentioned equations.The red line shows the modification. Closed loop transfer function of ROGI controller is given by,

$$G_{mr}(s) = \frac{k_r + jk'_r}{(s - j\omega') + k_r + jk'_r} \tag{4.24}$$

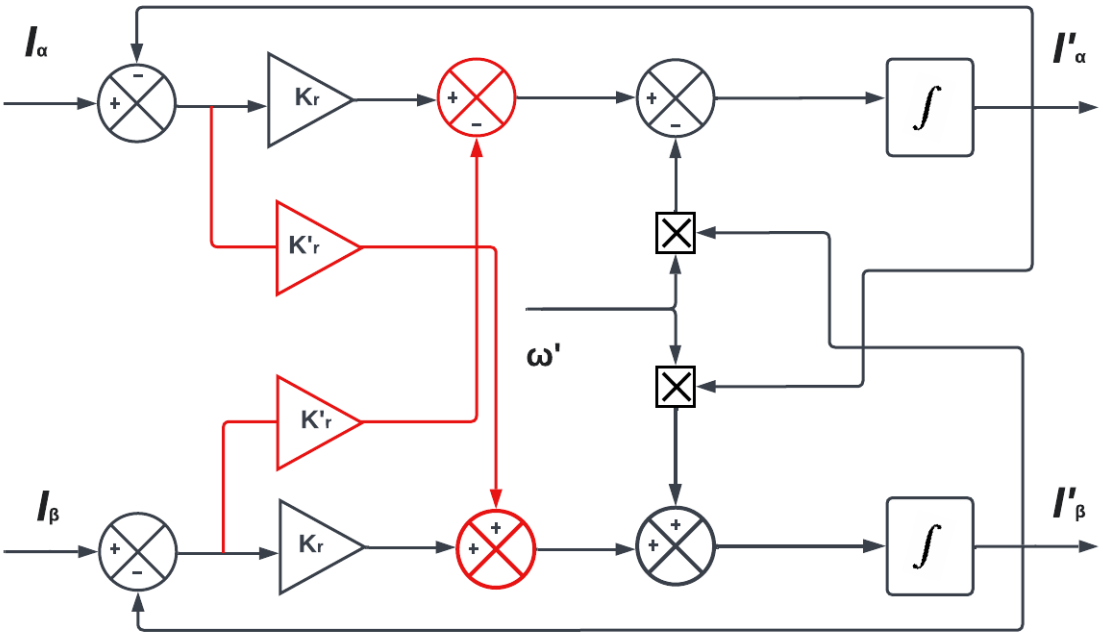

Figure 4.6: Basic Structure of Modified Reduced Order Generalized Integrator.

4.5 PI+Reduced Order Generalized Integrator

To increase performance, PI controller is added to the regular ROGI controller. The PI controller act as the feed-forward controller. Figure 4.7 illustrates the PI+ROGI controller's fundamental structure. The PI controller addition is indicated by the blue line. The PI+ROGI controller's transfer function is given by,

$$G_pr(s) = k_p + \frac{k_i}{s} + \frac{k_r}{(s - j\omega') + k_r} \tag{4.25}$$

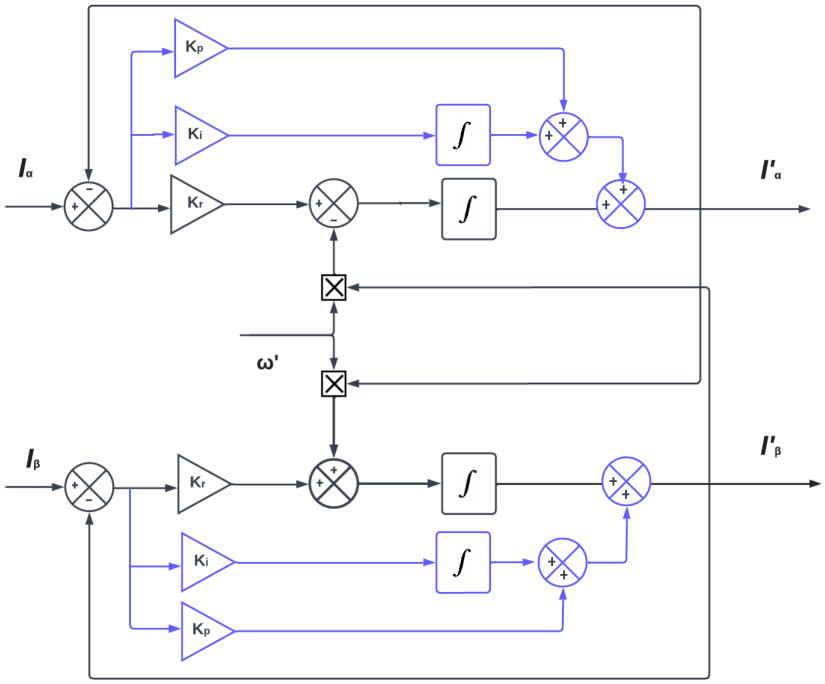

Figure 4.7: Basic Structure of PI+Reduced Order Generalized Integrator.

4.6 PI+Modified Reduced Order Generalized Integrator

The MROGI controller's performance is enhanced by the addition of a PI controller, creating the PI+MROGI controller. It provides a faster response time than MROGI controller. Figure 4.8 shows the basic structure of PI+MROGI. The blue line shows the addition of PI controller and the red line shows the modification from standard ROGI controller. The closed loop transfer function of PI+MROGI controller is given by,

$$G(s) = k_p + \frac{k_i}{s} + \frac{k_r + jk'_r}{(s - j\omega') + k_r + jk'_r} \tag{4.26}$$

where,

k_p=Proportional gain

k_i=Integral gain

The following formulas can be used to determine the current's amplitude and phase:

$$I' = \sqrt{{I'_\alpha}^2 + {I'_\beta}^2} \tag{4.27}$$

$$\theta' = tan^{-1}\left(\frac{I'_\beta}{I'_\alpha}\right) \tag{4.28}$$

where,

I'= Current Amplitude

θ'= Current Phase

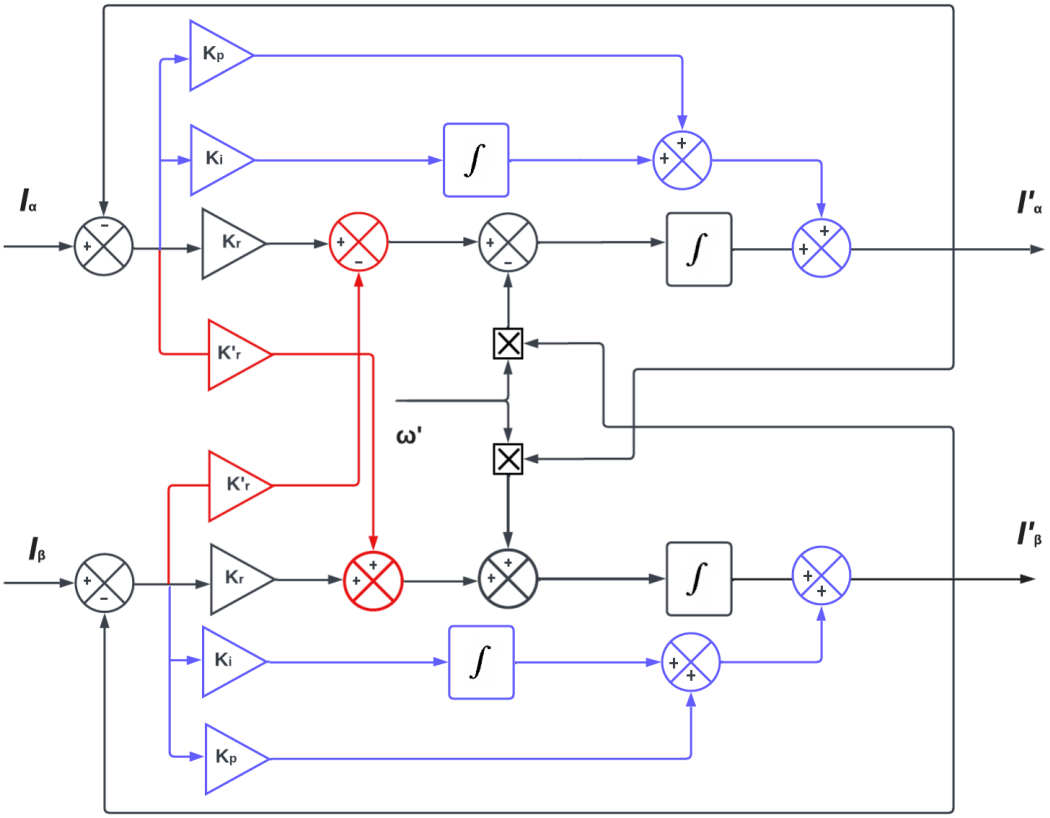

Figure 4.8: Basic Structure of PI+Modified Reduced Order Generalized Integrator.

4.7 Reference Current Generation

We must determine the reference current to generate the gate pulse for the inverter after extracting the fundamental component of the load current using the above controllers. In order to do it, grid voltages at Point of Common Coupling(PCC) are sensed and is used to calculate the Unit Vector Template V_t.

$$V_t = \sqrt{0.666\left(v_{pa}^2 + v_{pb}^2 + v_{pc}^2\right)} \tag{4.29}$$

where, V_{pa}, V_{pb} and V_{pc} are the sensed grid voltages at PCC.

The grid voltage's in-phase component is determined using,

$$\begin{cases} v_{ia} = \dfrac{v_{pa}}{V_t}, \\ v_{ib} = \dfrac{v_{pb}}{V_t}, \\ v_{ic} = \dfrac{v_{pc}}{V_t} \end{cases} \tag{4.30}$$

Calculating the quadrature component of UVT involves,

$$\begin{cases} v_{qa} = \dfrac{v_{ic}}{1.732} - \dfrac{v_{ib}}{1.732}, \\ v_{qb} = \dfrac{1.732.v_{ia}}{2} - \dfrac{(v_{ib} - v_{ic})}{3.464}, \\ v_{qc} = -\dfrac{1.732.v_{ia}}{2} - \dfrac{(v_{ib} - v_{ic})}{3.464} \end{cases} \tag{4.31}$$

To create active power constituents (I_a, I_b, I_c) of the load current, the extracted fundamental load current constituents are sampled and hold at the Zero Crossing Detection (ZCD) unit with UVT quadrature constituents.

Utilizing hybrid system current at the DC link I_{hsff}, active power components (I_a, I_b, I_c), and current loss of the DC link regulator I_{loss}, the net load current constituents are determined by,

$$i_{net} = \frac{i_a + i_b + i_c - i_{hsff} + i_{loss}}{3} \tag{4.32}$$

Current loss of the DC link regulator, I_{loss} can be obtained by using a Proportional-Integral-Derivative (PID) controller.

$$I_{\text{loss}} = \frac{1}{3}\left(V_{dcref} - V_{dcact}\right)\left(K_p + \frac{K_i}{s} + K_d(s)\right) \tag{4.33}$$

where,

V_{dcref}= DC reference voltage

V_{dcact}= Actual DC voltage

k_p,,k_i,k_d= PID controller gain

$$I_{hsff} = \frac{P_{hs}}{V_t} \tag{4.34}$$

where, P_{hs} is the total power of hybrid system.

Using the fundamental net constituent current and in-phase UVT, reference currents (I_{ra}, I_{rb} and I_{rc}) are generated.

$$\begin{cases} i_{ra} = i_{net}.v_{ia}, \\ i_{rb} = i_{net}.v_{ib}, \\ i_{rc} = i_{net}.v_{ic} \end{cases} \tag{4.35}$$

To create the three-phase anti-harmonic current, the calculated reference currents are compared to the true grid current. The pulses needed by the inverter to inject the anti-harmonic current into the utility grid are produced by a PWM controller. Current harmonics are corrected in this way.

4.8 Conclusion

This chapter discussed about the overall design of the different controllers used for reducing the harmonics of the grid current, and the reference current generation method.

Chapter 5

SIMULATION RESULTS

5.1 Introduction

This chapter tests the controller's efficiency in reducing harmonics using simulations in both PV systems and hybrid systems.

5.2 Open Loop Simulation Result

When a nonlinear load is coupled to a grid, the grid voltage and current will mirror the harmonic-containing nonlinear load current[24]. Figure 5.1 displays the output voltage and current for the load, while Figure 5.2 displays the output voltage and current for the grid without a controller. Using Fast Fourier Transform (FFT) analysis, it was discovered that the grid current's Total Harmonic Distortion (THD) is 20.70%. THD is a measurement of how much the ideal waveform of the power supplied by your utility is distorted by your load. THD levels of no more than 5% are advised by IEEE 519. As a result, THD needs to be decreased to a reasonable level. As a result, various controllers are used in both PV integrated system and a hybrid system.

The load current with harmonic content is filtered using various control techniques, and anti-harmonic current is then injected into the utility grid in order to remove the harmonics.By sending pulses to the inverter, the anti-harmonic current in a renewable energy integrated system can be fed into the utility grid.

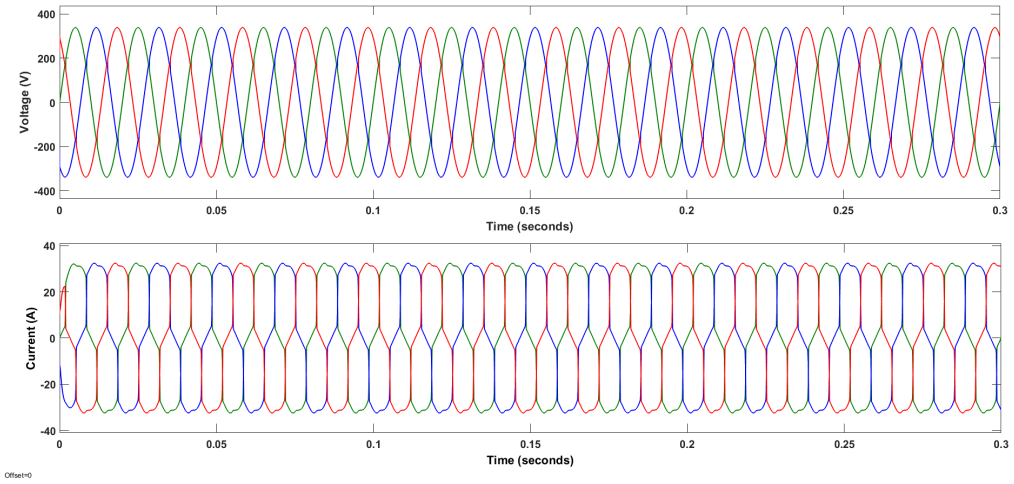

Figure 5.1: Simulation result of load voltage and current.

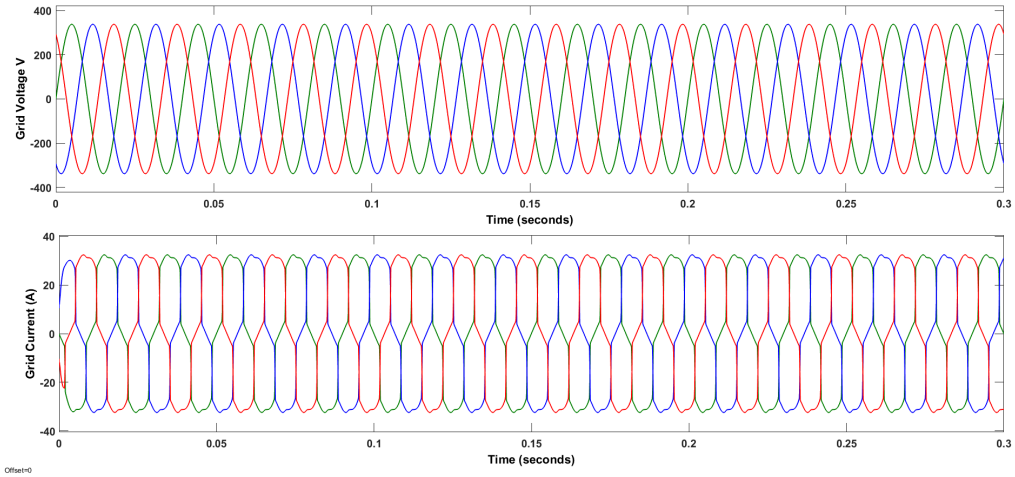

Figure 5.2: Simulation result of grid voltage and current before controller is used.

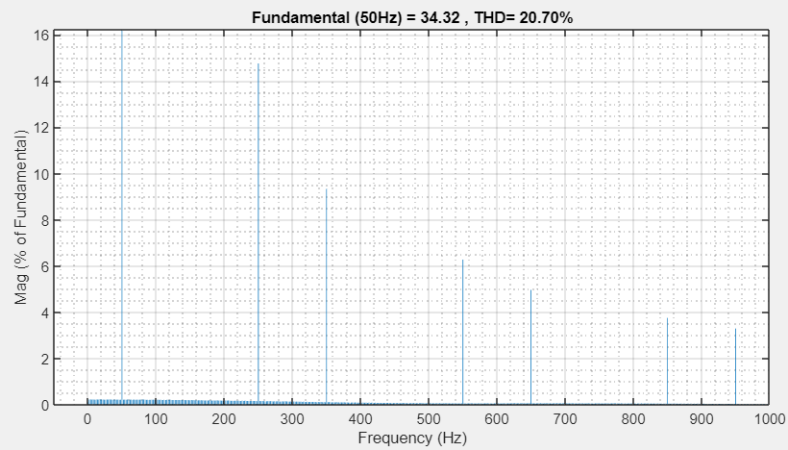

Figure 5.3: THD of grid current before controller is used.

5.3 Performance of Various Controllers in PV Integrated System - Simulink Results

A PV integrated system is first taken into account. Figure 5.4 depicts the PV output waveform and DC link voltage. PV generates an output voltage,V_{PV} of 500 V and current,I_{PV} of 63A. The output power,P_{PV} is constant and is 35kW. A boost converter is then supplied with this voltage.

The input of the inverter must be a constant DC voltage for the proper functioning of the controller. 800 V is the output DC link capacitor voltage,V_{dc}. This DC link voltage is delivered into the inverter's input.

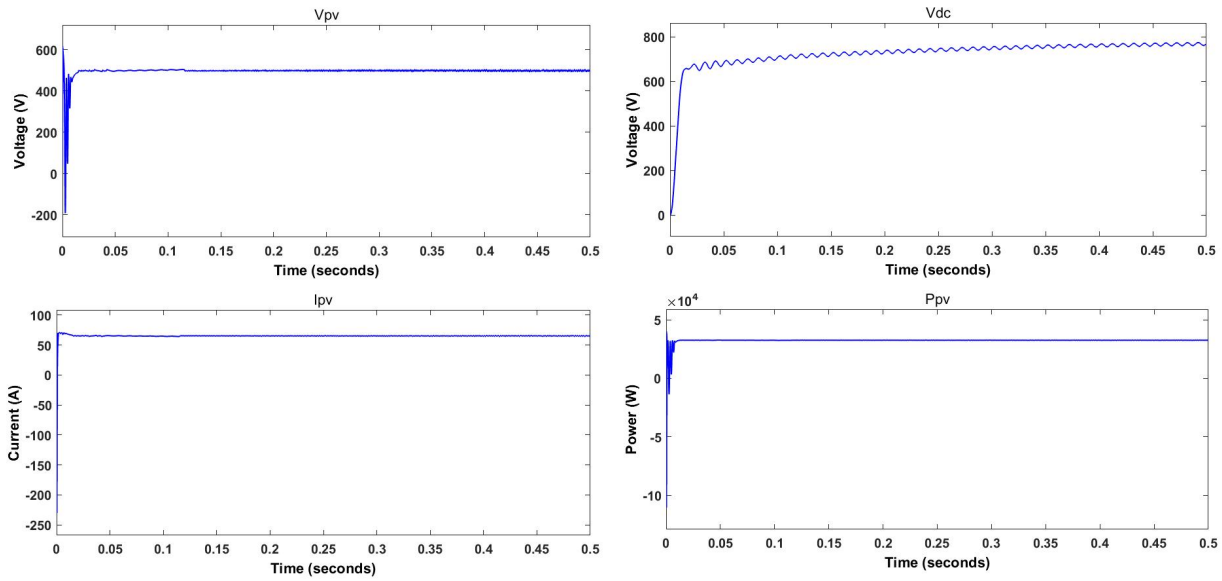

Figure 5.4: Output PV Waveform and DC-link Voltage

The following sections provide the grid voltage and current output waveform utilising various controllers. THD of the grid current is also estimated using FFT analysis. DC offset, third and fifth harmonics is also computed and is compared.

5.3.1 DSOGI Controller

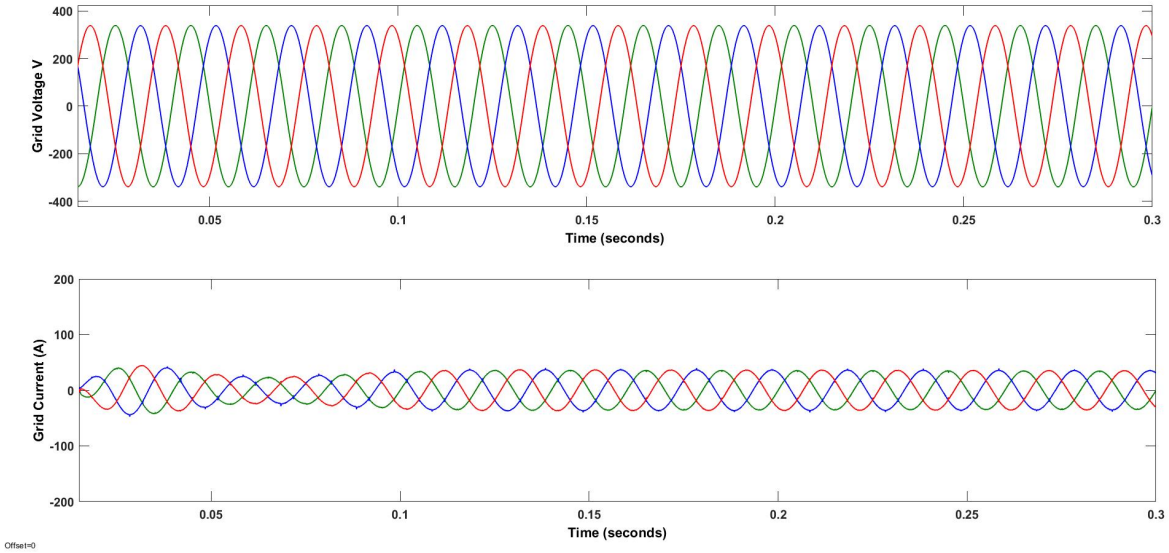

Figure 5.5: Simulation result of compensated grid voltage and current after using DSOGI controller.

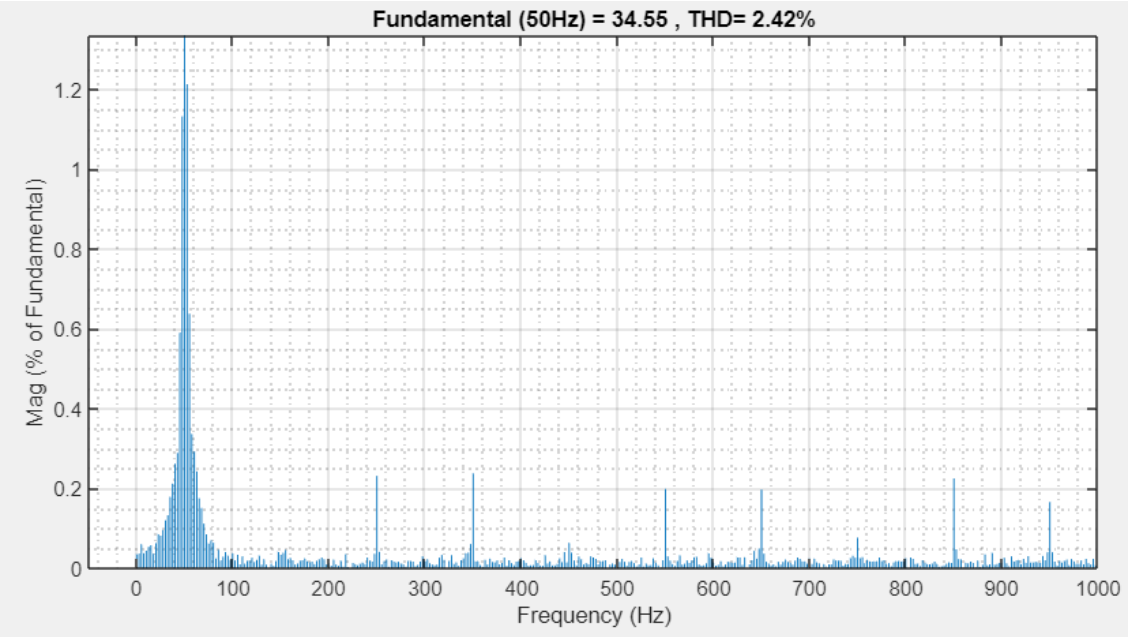

Figure 5.6: THD of grid current after using DSOGI controller.

Figure 5.5 shows the grid voltage and current after utilising a DSOGI controller. THD is 2.42% after using this controller. Harmonic content has been decreased and is now within IEEE's permitted range.

5.3.2 ROGI Controller

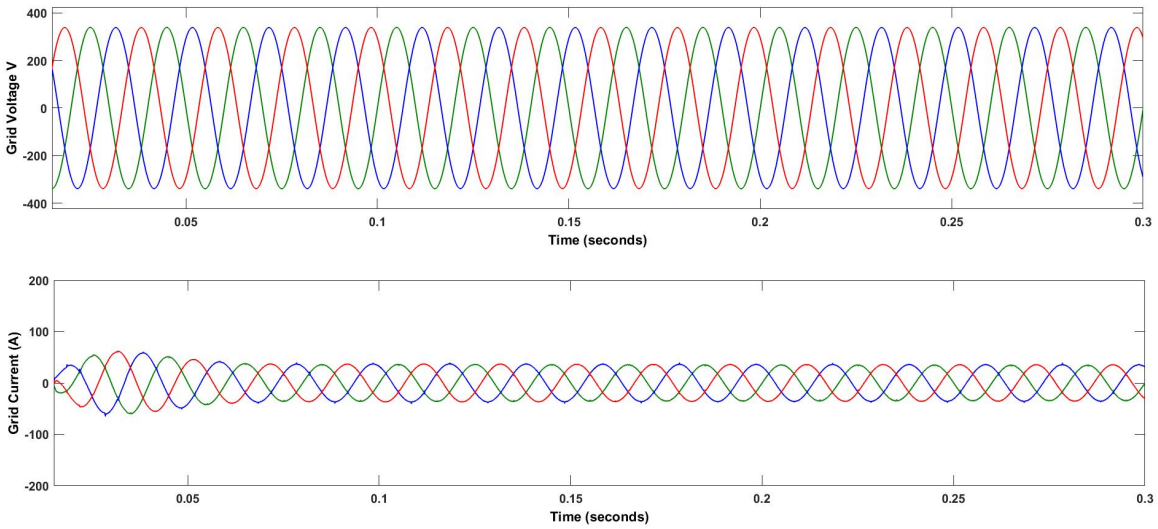

Figure 5.7: Simulation result of compensated grid voltage and current after using ROGI controller.

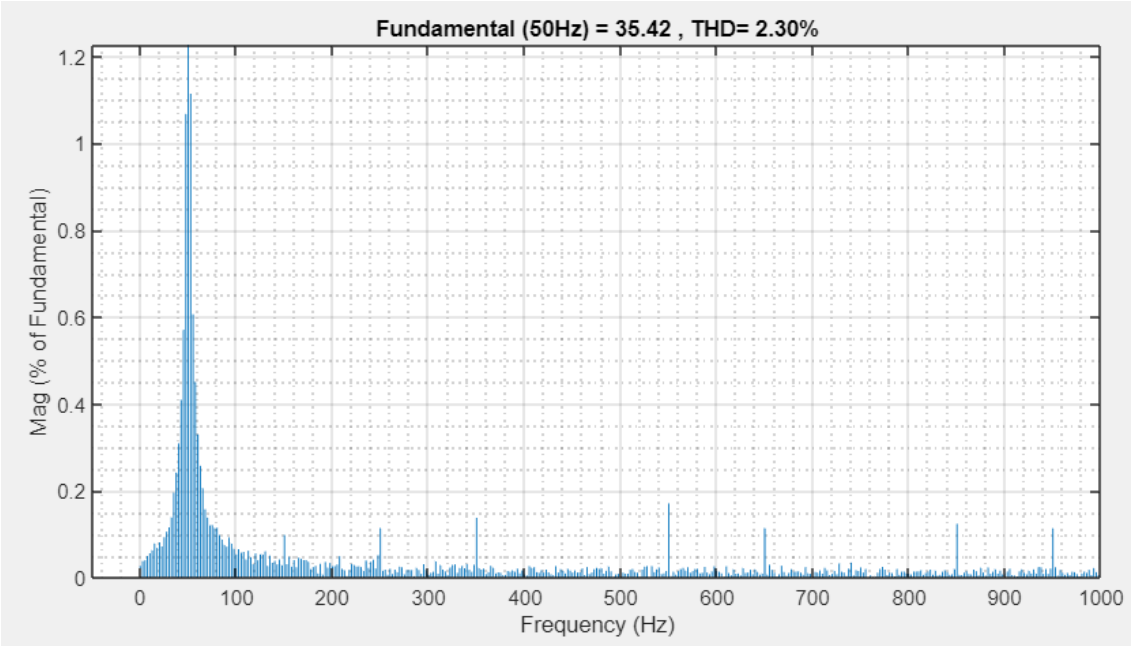

Figure 5.8: THD of grid current after using ROGI controller.

Figure 5.7 shows the grid voltage and current after utilising a ROGI controller. THD is 2.30% after using this controller. Harmonic content has been decreased and is within IEEE's permitted range.

5.3.3 MROGI Controller

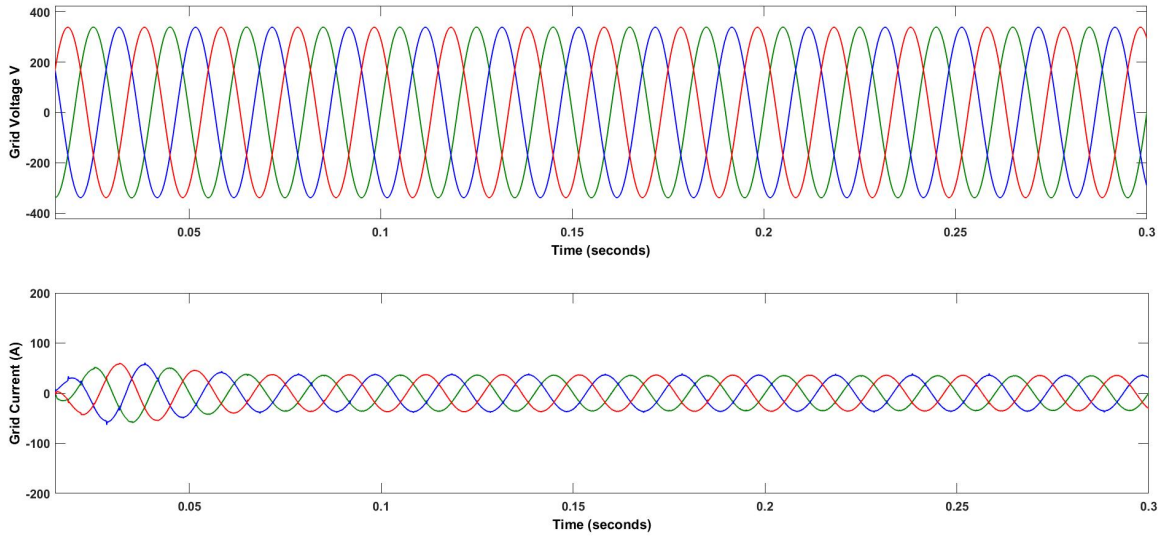

Figure 5.9: Simulation result of compensated grid voltage and current after using MROGI controller.

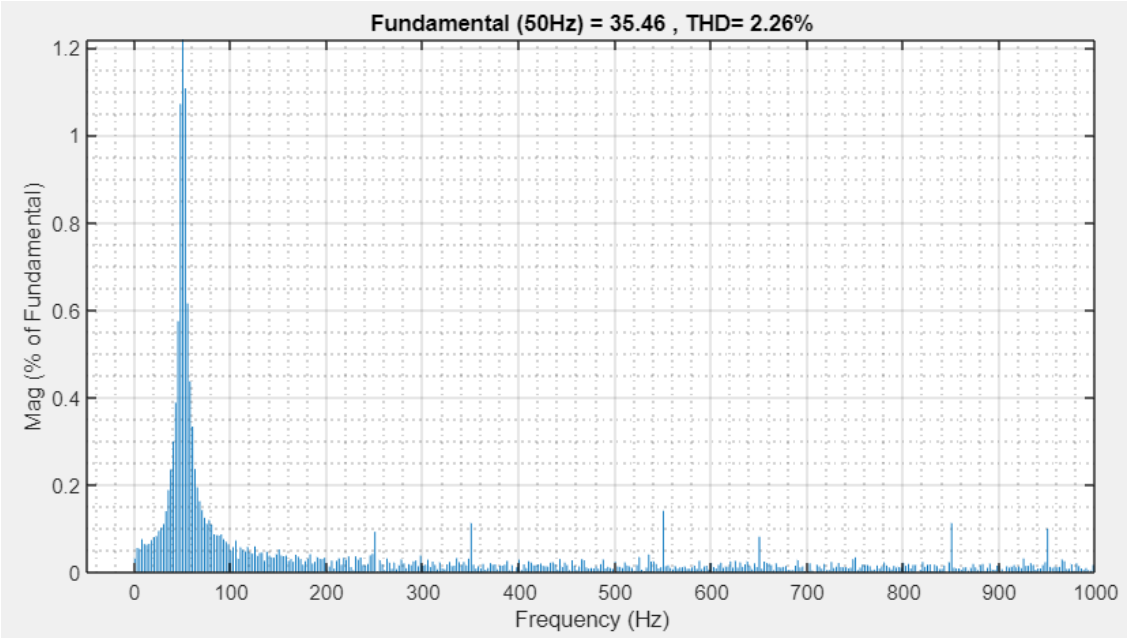

Figure 5.10: THD of grid current after using MROGI controller.

Figure 5.9 shows the grid voltage and current after utilising a MROGI controller. THD is 2.26% after using this controller. Harmonic content has been decreased and is within IEEE's permitted range.

5.3.4 PIROGI Controller

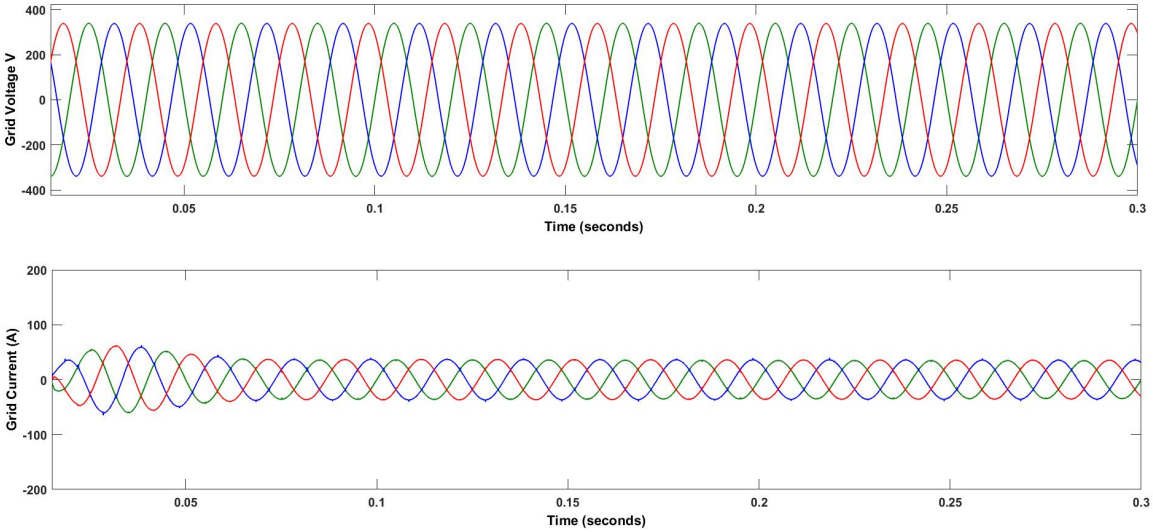

Figure 5.11: Simulation result of compensated grid voltage and current after using PIROGI controller.

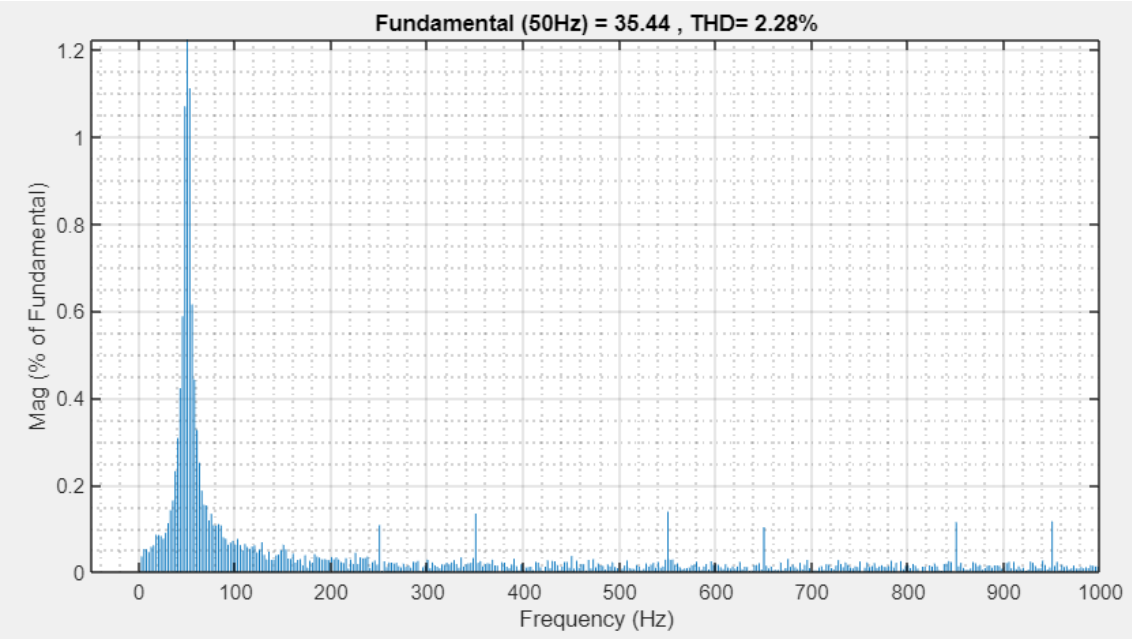

Figure 5.12: THD of grid current after using PIROGI controller.

Figure 5.11 shows the grid voltage and current after utilising a PIROGI controller. THD is 2.28% after using this controller. Harmonic content has been decreased and is within IEEE's permitted range.

5.3.5 PIMROGI Controller

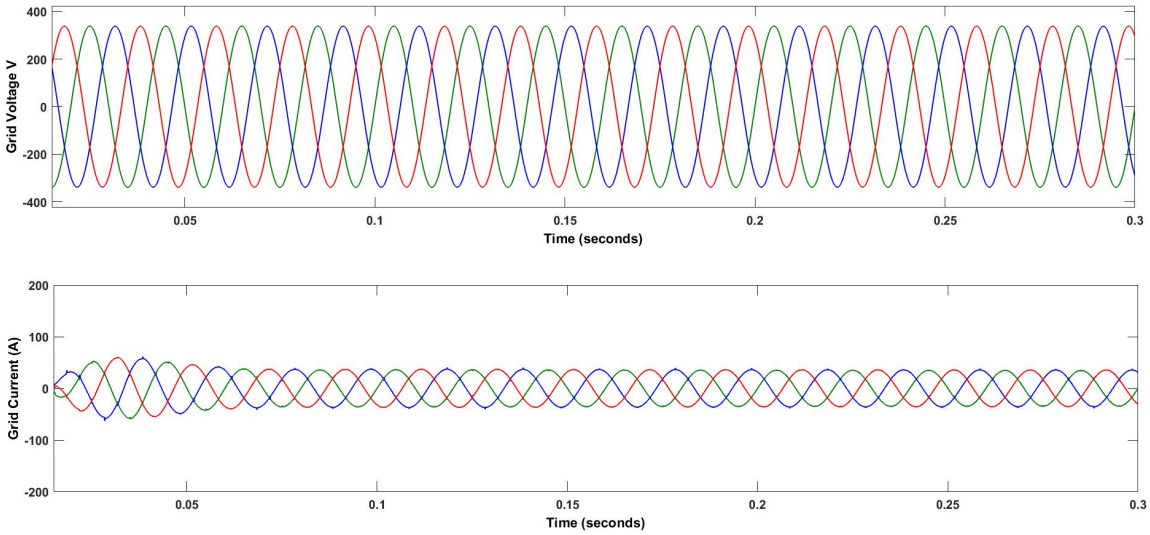

Figure 5.13: Simulation result of compensated grid voltage and current after using PIMROGI controller.

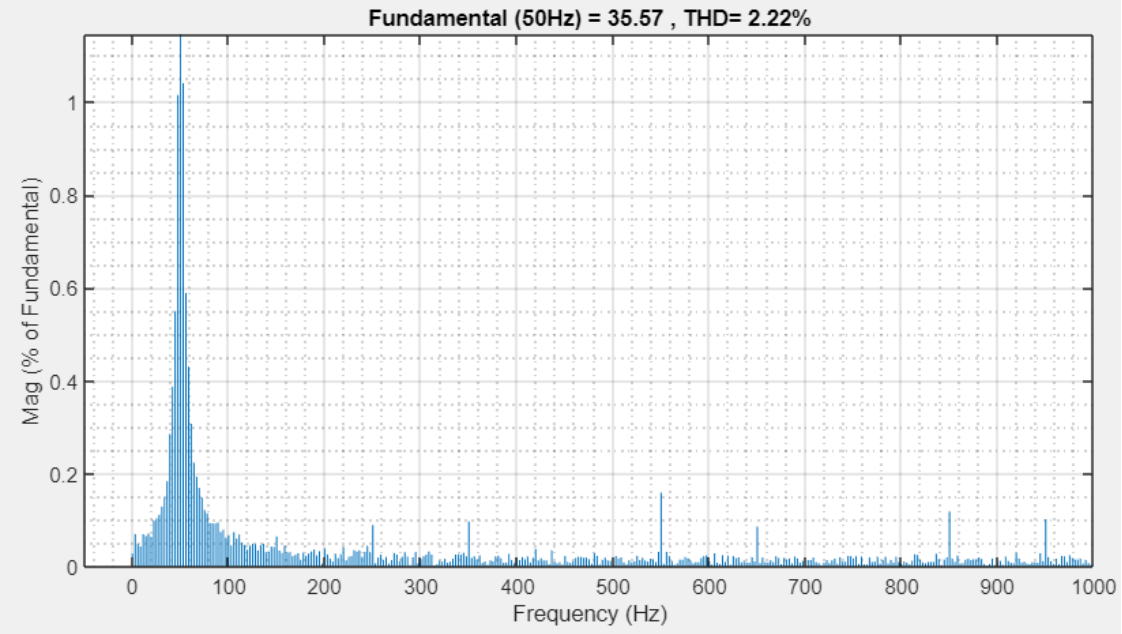

Figure 5.14: THD of grid current after using PIMROGI controller.

Figure 5.13 shows the grid voltage and current after utilising a PIMROGI controller. THD is 2.22% after using this controller. Harmonic content has been decreased and is within IEEE's permitted range.

5.3.6 Analysis of Result

Table 5.1: Comparison of the Harmonic compensation by different controllers in a PV-integrated system.

Controller	Magnitude (A)	Settling Time (s)	THD%	DC offset%	3^{rd} Harmonics%	5^{th} Harmonics%
DSOGI	34.55	0.125	2.42	0.04	0.03	0.23
ROGI	35.42	0.06	2.30	0.03	0.1	0.11
PIROGI	35.44	0.05	2.28	0.02	0.06	0.11
MROGI	35.46	0.05	2.26	0.03	0.05	0.09
PIMROGI	35.57	0.04	2.22	0.03	0.06	0.09

5.4 Performance of Various Controllers in a Hybrid System - Simulink Results

The controllers are also analysed in a hybrid system. A fuel cell is connected in parallel with the PV. The output waveform of a PV is depicted in Figure 5.15, together with the DC link voltage. The output waveform of the fuel cell is depicted in Figure 5.16.

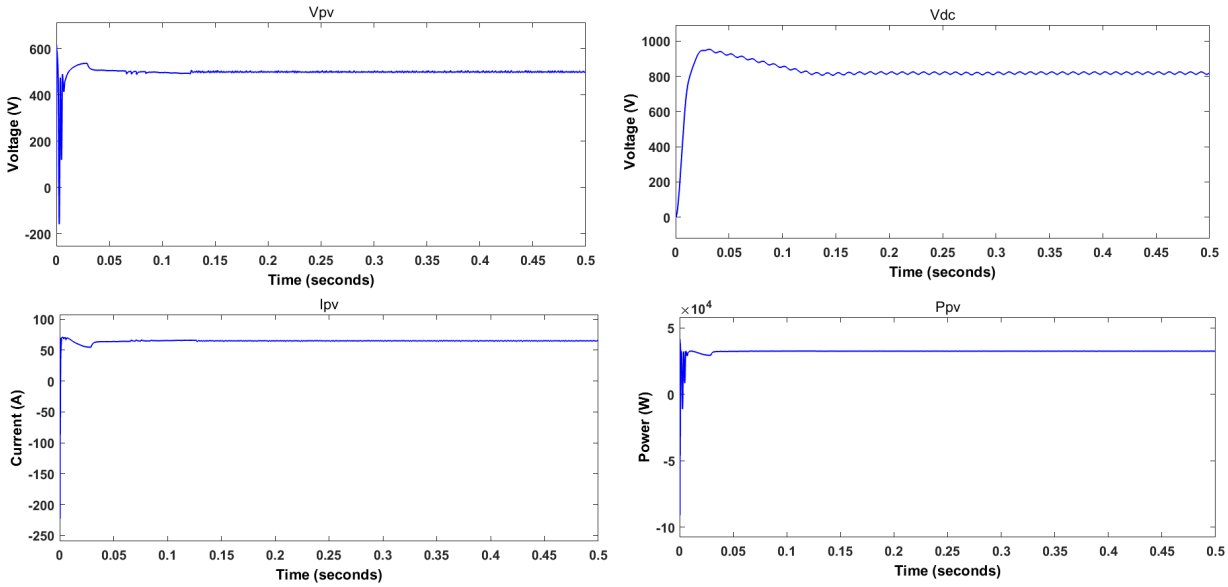

Figure 5.15: Output PV Waveform and DC-link Voltage

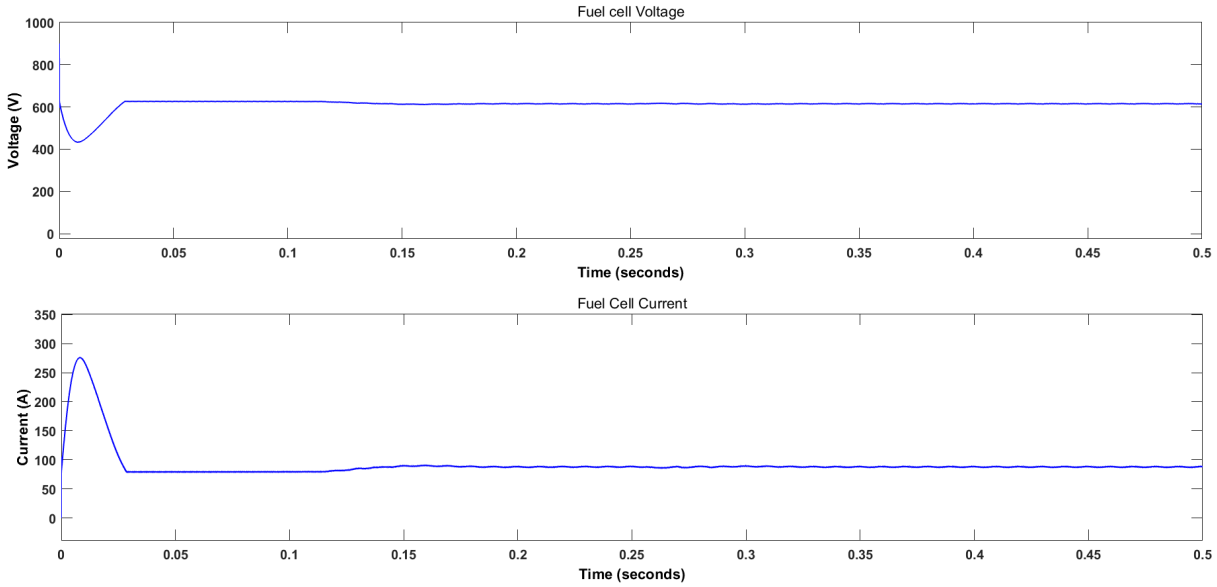

Figure 5.16: Output waveform of fuel cell

Figure 5.17 shows the output of Frequency Locked Loop. The frequency is maintained at 50Hz.

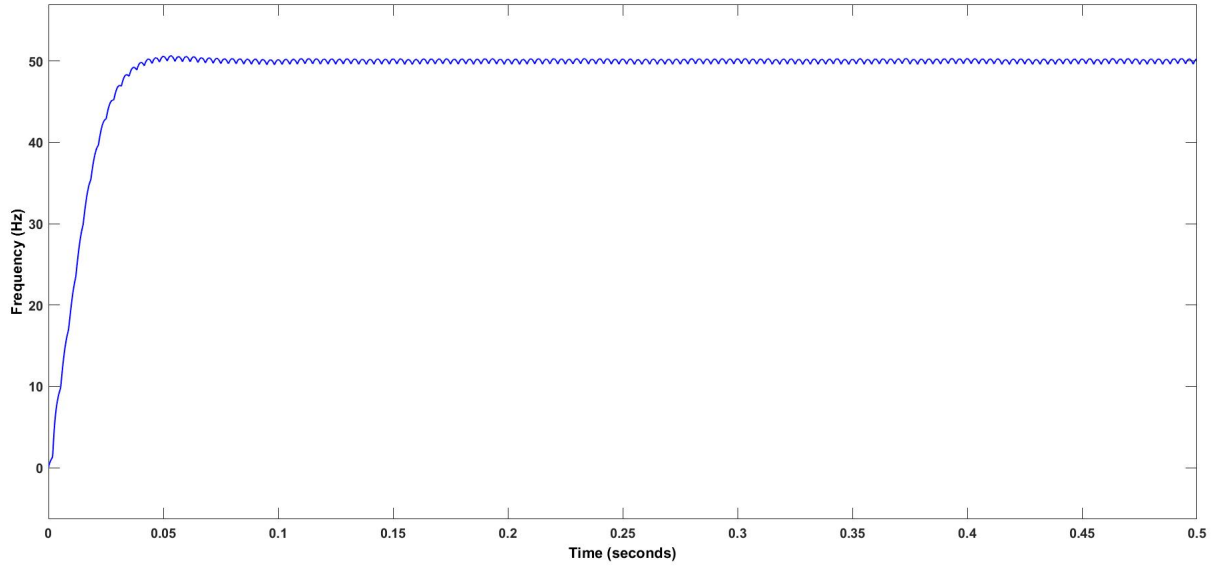

Figure 5.17: FLL Frequency

The following sections provide the grid voltage and current output waveform utilising various controllers. THD of the grid current is also estimated using FFT analysis. DC offset, third and fifth harmonics is also computed and is compared.

5.4.1 DSOGI Controller

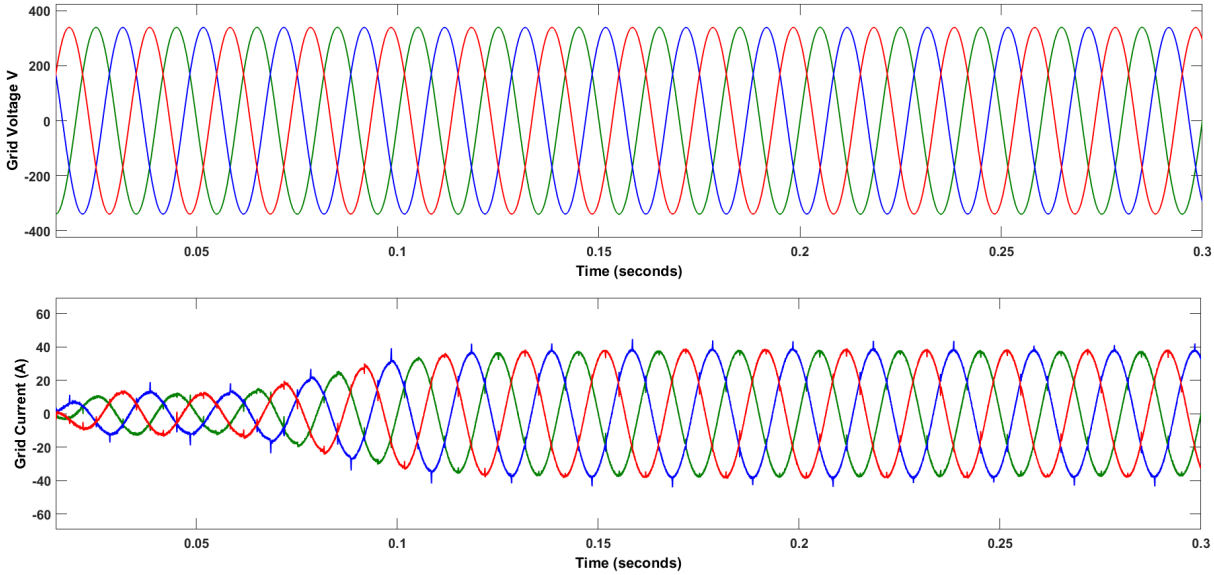

Figure 5.18: Simulation result of compensated grid voltage and current after using DSOGI controller.

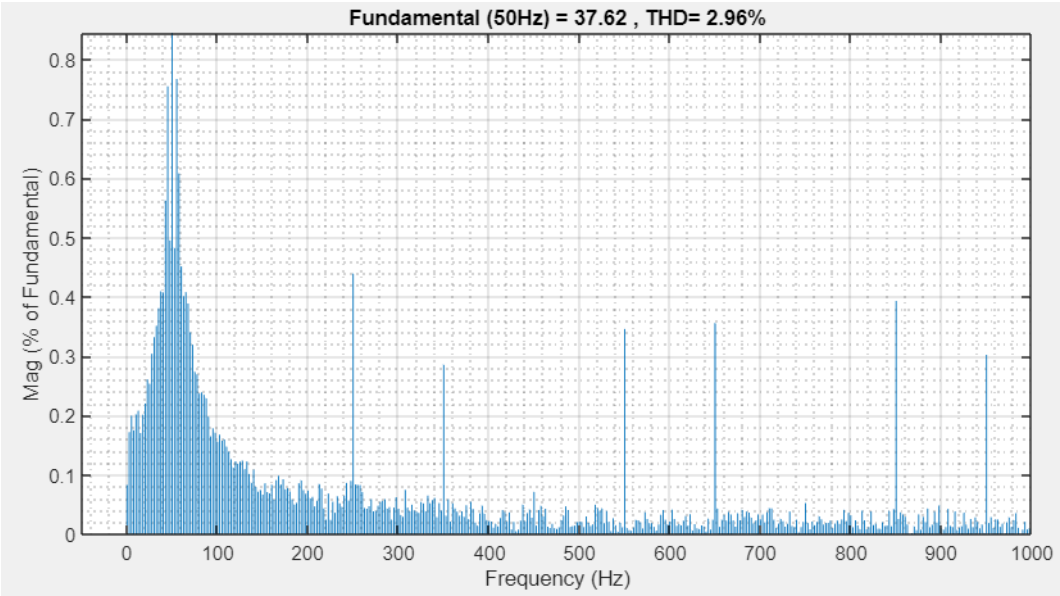

Figure 5.19: THD of grid current after using DSOGI controller.

Figure 5.18 shows the grid voltage and current after utilising a DSOGI controller. THD is 2.96% after using this controller. Harmonic content has been decreased and is now within IEEE's permitted range.

5.4.2 ROGI Controller

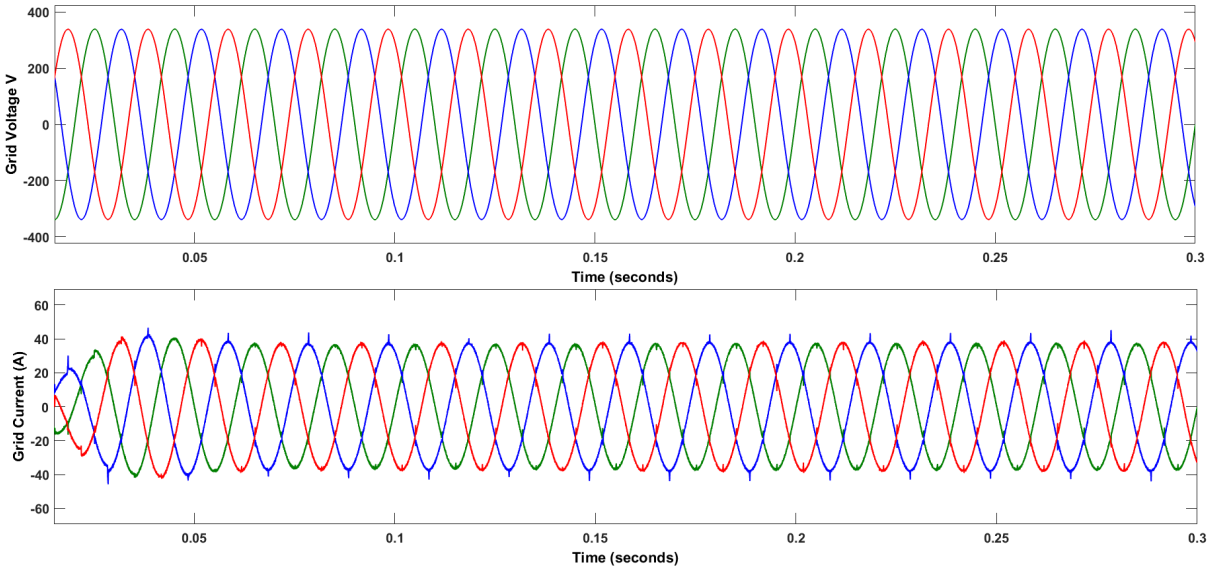

Figure 5.20: Simulation result of compensated grid voltage and current after using ROGI controller.

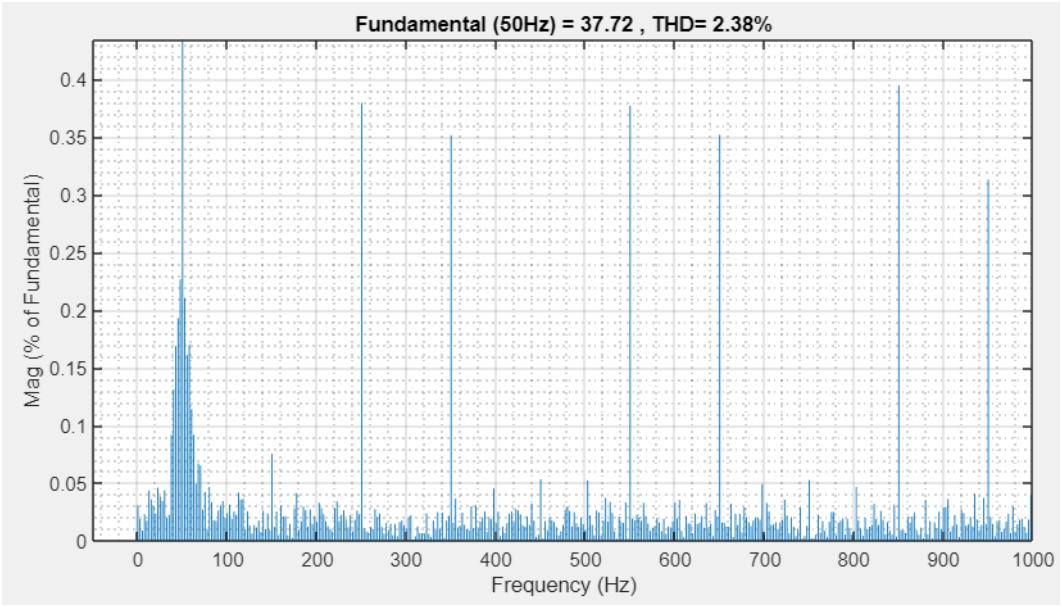

Figure 5.21: THD of grid current after using ROGI controller.

Figure 5.20 shows the grid voltage and current after utilising a ROGI controller. THD is 2.38% after using this controller. Harmonic content has been decreased and is within IEEE's permitted range.

5.4.3 MROGI Controller

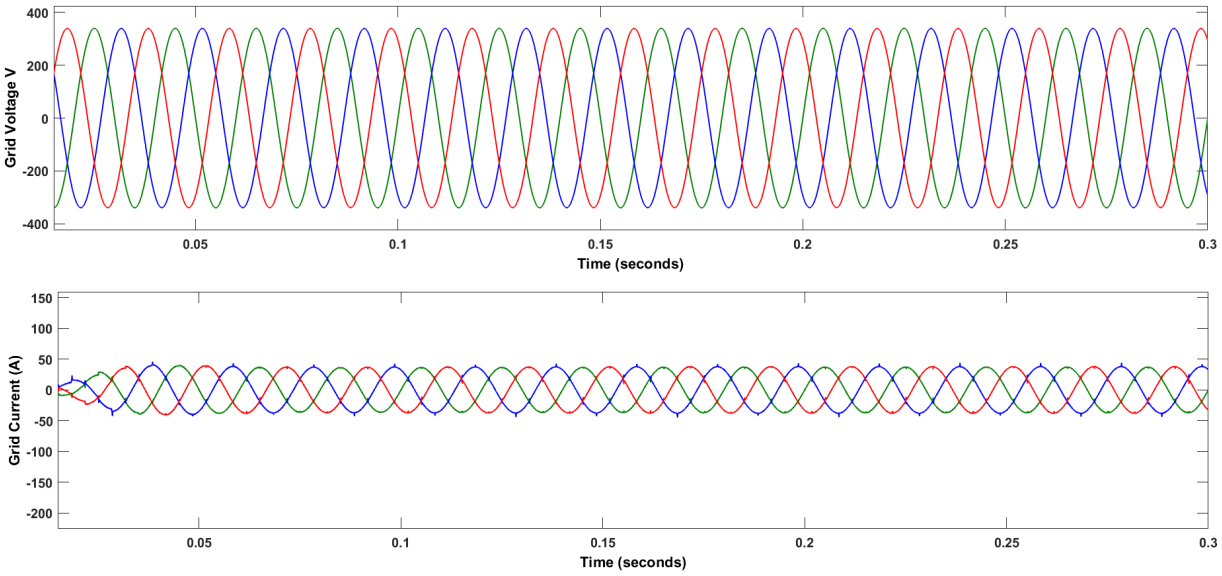

Figure 5.22: Simulation result of compensated grid voltage and current after using MROGI controller.

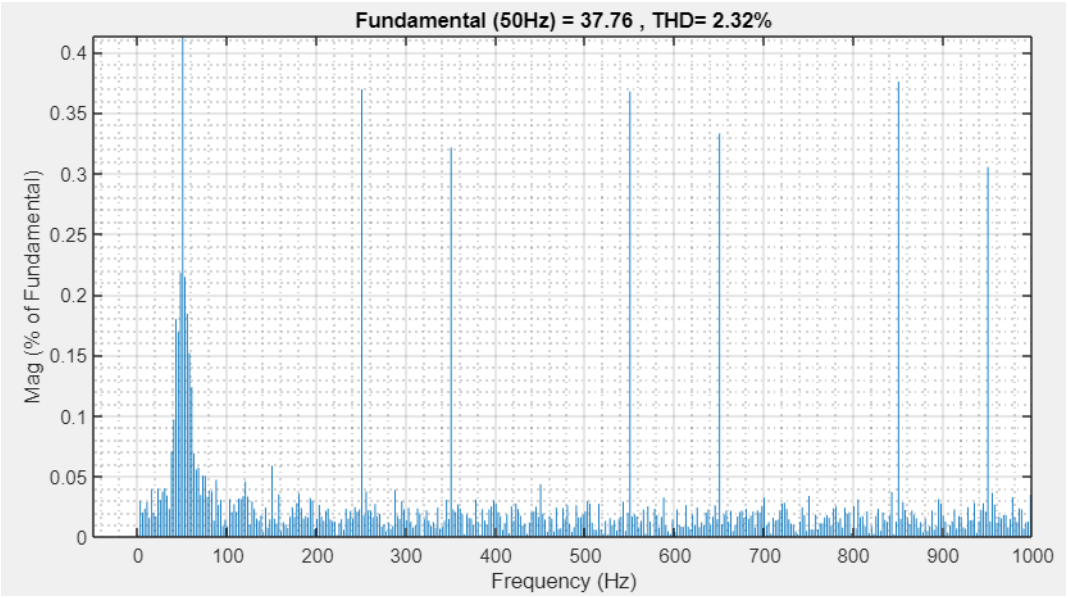

Figure 5.23: THD of grid current after using MROGI controller.

Figure 5.22 shows the grid voltage and current after utilising a MROGI controller. THD is 2.32% after using this controller. Harmonic content has been decreased and is within IEEE's permitted range.

5.4.4 PIROGI Controller

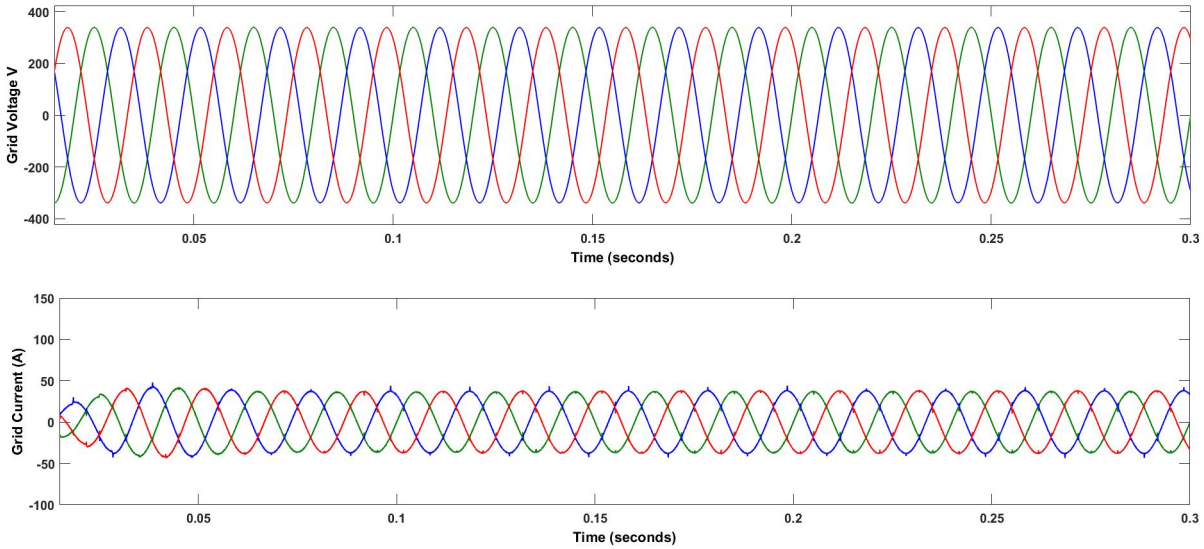

Figure 5.24: Simulation result of compensated grid voltage and current after using PIROGI controller.

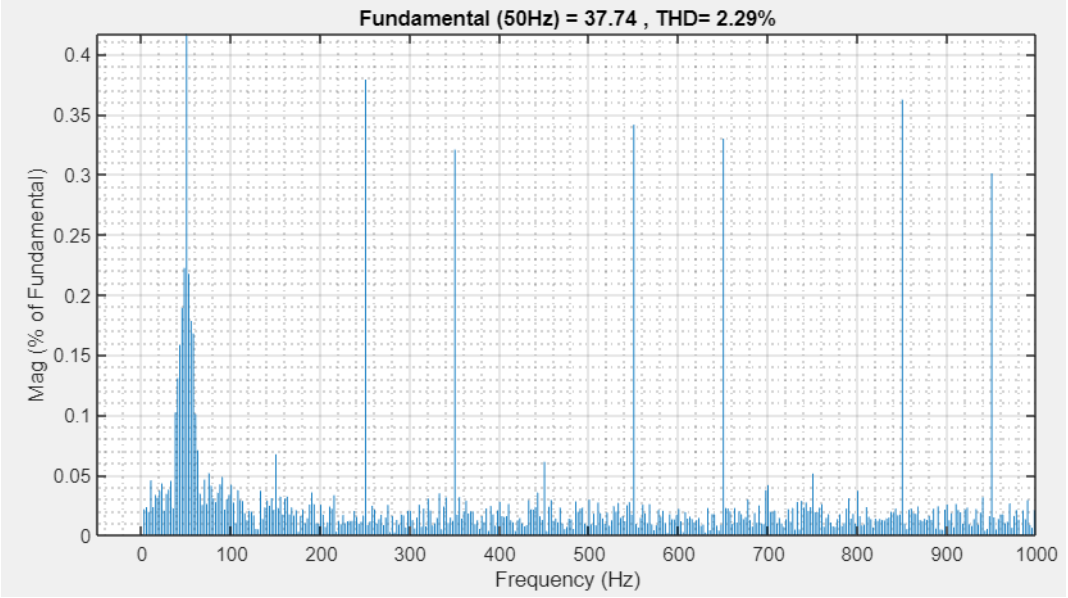

Figure 5.25: THD of grid current after using PIROGI controller.

Figure 5.24 shows the grid voltage and current after utilising a PIROGI controller. THD is 2.29% after using this controller. Harmonic content has been decreased and is within IEEE's permitted range.

5.4.5 PIMROGI Controller

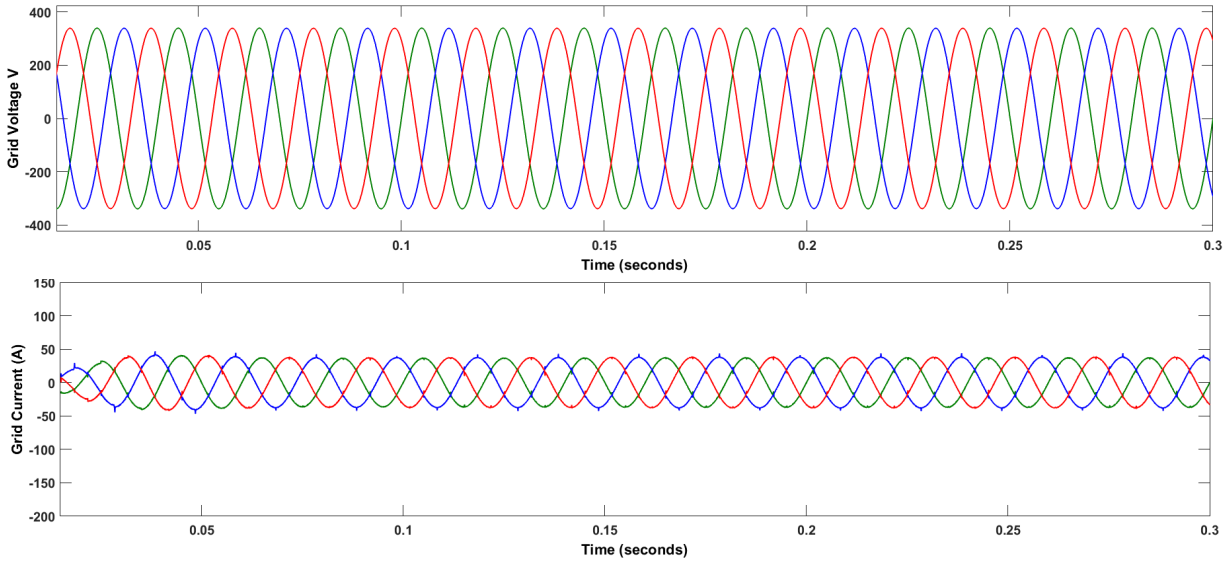

Figure 5.26: Simulation result of compensated grid voltage and current after using PIMROGI controller.

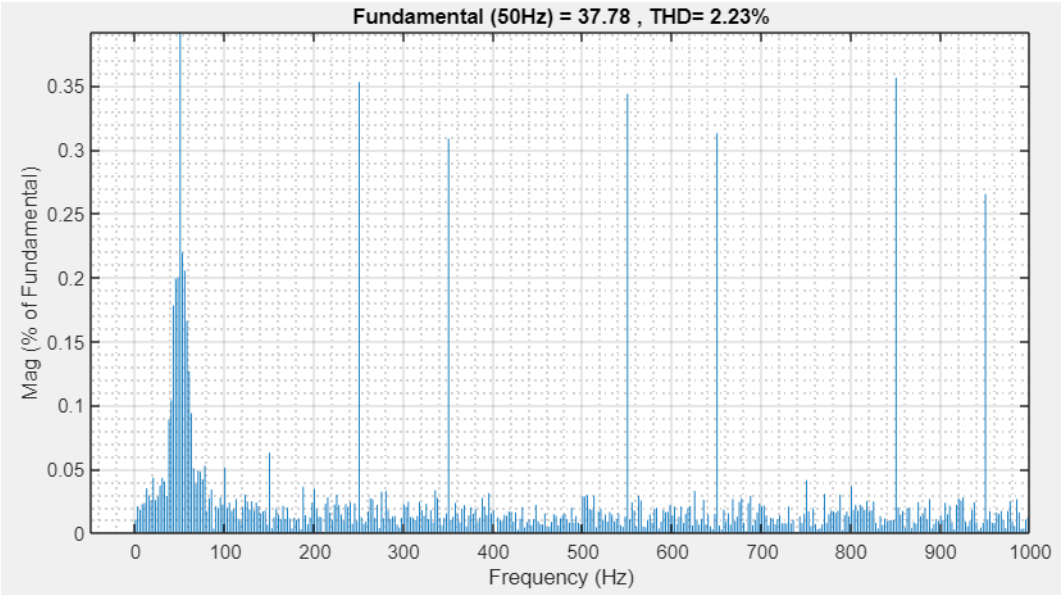

Figure 5.27: THD of grid current after using PIMROGI controller.

Figure 5.26 shows the grid voltage and current after utilising a PIMROGI controller. THD is 2.23% after using this controller. Harmonic content has been decreased and is within IEEE's permitted range.

5.4.6 Analysis of Results

Table 5.2: Comparison of the Harmonic compensation by different controllers in a hybrid system.

Controller	Magnitude (A)	Settling Time (s)	THD%	DC offset%	3^{rd} Harmonics%	5^{th} Harmonics%
DSOGI	37.62	0.125	2.96	0.08	0.07	0.44
ROGI	37.72	0.06	2.38	0.03	0.08	0.38
MROGI	37.76	0.05	2.32	0	0.06	0.37
PIROGI	37.74	0.05	2.29	0	0.07	0.38
PIMROGI	37.78	0.04	2.23	0	0.06	0.35

5.5 Conclusion

This chapter discussed about the simulation result of different controllers for harmonic compensation in both pv integrated system and a hybrid system.The performance of these controllers are analysed and compared. It is seen than PI+MROGI controller gives better results.

Chapter 6

CONCLUSION AND FUTURE SCOPE

In this study, a brand-new control strategy is put forth to efficiently reduce the harmonic currents that nonlinear loads connected to the grid produce. In addition to feedback control, the PI+MROGI-FLL controller also employs a feed forward PI controller. In order to control the imaginary part of the closed loop eigenvalues, it additionally employs a cross feedback control. This improves the performance of the proposed controller. By adaptively measuring the amplitude, frequency, and phase angle, the proposed control technique effectively corrected the grid harmonics. When the suggested controller's performance is compared to that of existing traditional controllers like DSOGI, ROGI, MROGI, and PI+ROGI, the proposed controller outperforms the others in mitigating harmonics.

The future scope of the work includes analysing the controller under imbalanced system voltage and system voltage sag and swell conditions.

References

[1] Wikipedia contributors, "Photovoltaic system — Wikipedia, the free encyclopedia," 2022. [Online; accessed 1-July-2022].

[2] Wikipedia contributors, "Proton-exchange membrane fuel cell — Wikipedia, the free encyclopedia," 2022. [Online; accessed 1-July-2022].

[3] X. Liang and C. Andalib-Bin-Karim, "Harmonics and mitigation techniques through advanced control in grid-connected renewable energy sources: A review," *IEEE Transactions on Industry Applications*, vol. 54, no. 4, pp. 3100–3111, 2018.

[4] P. Acuna, L. Moran, M. Rivera, J. Dixon, and J. Rodriguez, "Improved active power filter performance for renewable power generation systems," *IEEE transactions on power electronics*, vol. 29, no. 2, pp. 687–694, 2013.

[5] A. Kherbachi, A. Chouder, A. Bendib, K. Kara, and S. Barkat, "Enhanced structure of second-order generalized integrator frequency-locked loop suitable for dc-offset rejection in single-phase systems," *Electric Power Systems Research*, vol. 170, pp. 348–357, 2019.

[6] N. P. Babu, C. B. Babu, R. B. Peesapati, and G. Panda, "An optimal current control scheme in grid-tied hybrid energy system with active power filter for harmonic mitigation," *International Transactions on Electrical Energy Systems*, vol. 30, no. 3, 2020.

[7] S. Mandava, P. K. Medarametla, A. Gudipalli, M. Saravanan, and P. Sudheer, "Integration of ai with reduced order generalized integrator controller for power system harmonic reduction," *Computational Intelligence*, vol. 37, no. 3, pp. 1068–1079, 2021.

[8] M. Ramezani, S. Li, and S. Golestan, "Analysis and controller design for stand-alone vsis in synchronous reference frame," *IET Power Electronics*, vol. 10, no. 9, pp. 1003–1012, 2017.

[9] S. K. Chauhan, M. C. Shah, R. R. Tiwari, and P. Tekwani, "Analysis, design and digital implementation of a shunt active power filter with different schemes of reference current generation," *IET Power Electronics*, vol. 7, no. 3, pp. 627–639, 2014.

[10] Y. Hoon, M. A. M. Radzi, M. K. Hassan, and N. F. Mailah, "Operation of three-level inverter-based shunt active power filter under nonideal grid voltage conditions with dual fundamental component extraction," *IEEE Transactions on Power Electronics*, vol. 33, no. 9, pp. 7558–7570, 2017.

[11] S. Golestan, J. M. Guerrero, J. C. Vasquez, A. M. Abusorrah, and Y. Al-Turki, "Modeling, tuning, and performance comparison of second-order-generalized-integrator-based flls," *IEEE Transactions on Power Electronics*, vol. 33, no. 12, pp. 10229–10239, 2018.

[12] F. Xiao, L. Dong, L. Li, and X. Liao, "A frequency-fixed sogi-based pll for single-phase grid-connected converters," *IEEE Transactions on Power Electronics*, vol. 32, no. 3, pp. 1713–1719, 2016.

[13] F. Sevilmiş and H. Karaca, "Performance analysis of dual second order generalized integrator phase locked loop for grid interactive inverter," in *Proceedings of the 6th International Conference on Advanced Technology & Sciences (ICAT'Riga), Riga, Latvia*, pp. 12–15, 2017.

[14] C. A. Busada, S. G. Jorge, A. E. Leon, and J. A. Solsona, "Current controller based on reduced order generalized integrators for distributed generation systems," *IEEE Transactions on Industrial Electronics*, vol. 59, no. 7, pp. 2898–2909, 2011.

[15] A. J. Wang, B. Y. Ma, and C. X. Meng, "A frequency-locked loop technology of three-phase grid-connected inverter based on improved reduced order generalized integrator," in *2015 IEEE 10th conference on industrial electronics and applications (ICIEA)*, pp. 730–735, IEEE, 2015.

[16] N. Babu, J. M. Guerrero, P. Siano, R. Peesapati, and G. Panda, "A novel modified control scheme in grid-tied photovoltaic system for power quality enhancement," *IEEE Transactions on Industrial Electronics*, vol. 68, no. 11, pp. 11100–11110, 2020.

[17] P. V. Patel, *Modeling and control of three-phase grid-connected PV inverters in the presence of grid faults*. Missouri University of Science and Technology, 2018.

[18] B. Singh, C. Jain, and S. Goel, "Ilst control algorithm of single-stage dual purpose grid connected solar pv system," *IEEE Transactions on Power Electronics*, vol. 29, no. 10, pp. 5347–5357, 2013.

[19] A. Y. Abdelaziz, A. M. Atallah, and R. S. Jumaah, "Modeling and simulation of a three-phase two-stage grid connected photovoltaic system," *no. September*, vol. 2013, 2015.

[20] G. Bayrak and M. Cebeci, "Grid connected fuel cell and pv hybrid power generating system design with matlab simulink," *International journal of hydrogen energy*, vol. 39, no. 16, pp. 8803–8812, 2014.

[21] M. I. Mosaad and H. Ramadan, "Power quality enhancement of grid-connected fuel cell using evolutionary computing techniques," *International Journal of Hydrogen Energy*, vol. 43, no. 25, pp. 11568–11582, 2018.

[22] H. A. Azzeddine, D.-E. Chaouch, M. Berka, M. Hebali, A. Larbaoui, and M. Tioursi, "Fuel cell grid connected system with active power generation and reactive power compensation features," *Przegląd Elektrotechniczny*, vol. 96, no. 11, pp. 124–127, 2020.

[23] E. Ozsoy, S. Padmanaban, F. Blaabjerg, P. Siano, F. Ahmad, R. Akhtar, and A. Sabanovic, "Digital application of second order generalized integrator based grid estimator under unbalanced and distorted voltage conditions," *Electric Power Components and Systems*, vol. 47, no. 16-17, pp. 1464–1474, 2019.

[24] S. Gomez Jorge, C. A. Busada, and J. Solsona, "Reduced order generalised integrator-based current controller applied to shunt active power filters," *IET Power Electronics*, vol. 7, no. 5, pp. 1083–1091, 2014.

List of Publications

[1] Sreelekshmi S, Thasneem A and Dr. Mathew P Abraham, "A Novel Control Scheme for Harmonic Compensation in PV-Integrated System," communicated to *International Conference on Edge Computing and Applications (ICECAA)*, 2022.

[2] Sreelekshmi S, Thasneem A and Dr. Mathew P Abraham, "A Novel Control Scheme for Harmonic Compensation in Hybrid System," communicated to *IEEE 19th India Council International Conference (INDICON)*, 2022.